Table of Contents Synopsis

Vanadium (V) complexes of a tripodal ligand, their characterisation and biological implications

M.R. Maurya, B. Uprety, F. Avecilla, P. Adão, and J. Costa Pessoa

Different vanadium(V) complexes with 6,6'–(2–(pyridin–2 yl)ethylazanediyl)bis(methylene) bis(2,4–di–tert–butylphenol) (H$_2$L^1) are isolated, characterized and one of them, [V^{V}O(OMe)(MeOH)(L^1)], is used as catalyst precursor as functional mimic of catechol–oxidase and for the oxidative bromination of thymol.
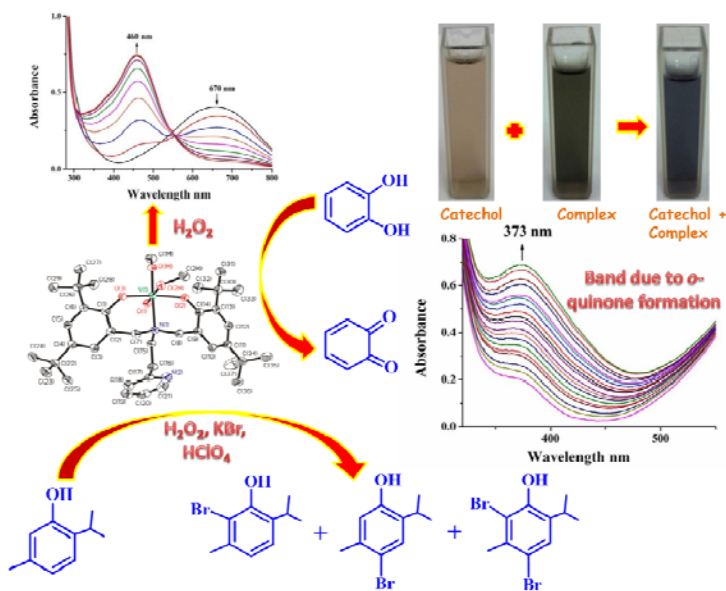
Vanadium (V) complexes of a tripodal ligand, their characterisation and biological implications†

Mannar R. Maurya,*[a] Bhawna Uprety,[a] Fernando Avecilla,[b] Pedro Adão,[c] and J. Costa Pessoa*[c]

[a] Department of Chemistry, Indian Institute of Technology Roorkee, Roorkee–247667, India. E–mail: rkmanfcy@iitr.ernet.in; Fax: +91 1332 273560; Tel: +91 1332 285327

[b] Departamento de Química Fundamental, Universidade da Coruña, Campus de A Zapateira, 15071 A Coruña, Spain

[c] Centro de Química Estrutural, Instituto Superior Técnico, Universidade Lisboa, 1049–001 Lisboa, Portugal. E–mail: joao.pessoa@ist.utl.pt; Fax: +351 21 8464455; Tel: +351 21 8419268

Abstract

The reaction of the tripodal tetradentate dibasic ligand 6,6'–(2–(pyridin–2–yl)ethylazanediyl)bis(methylene)bis(2,4–di–*tert*–butylphenol), H_2L^1 **I**, with $[V^{IV}O(acac)_2]$ in CH_3CN gives the V^VO–complex, $[V^VO(acac)(L^1)]$ **1**. Crystallisation of **1** in CH_3CN at ~0 ºC, gives dark blue crystals of **1**, while at room temperature it affords dark green crystals of $[\{V^VO(L^1)\}_2\mu–O]$ **3**. Upon prolonged treatment of **1** in MeOH $[V^VO(OMe)(MeOH)(L^1)]$ **2** is obtained. All three complexes are analysed by single–crystal X–ray diffraction, depicting distorted octahedral geometry around vanadium. In the reaction of H_2L^1 with $V^{IV}OSO_4$ partial hydrolysis of the tripodal ligand results in elimination of the pyridyl fragment of L^1 and the formation of $H[V^VO_2(L^2)]$ **4**, containing the ONO tridentate ligand 6,6'–azanediylbis(methylene)bis(2,4–di–*tert*–butylphenol), H_2L^2 **II**. Compound **4**, which was not fully characterised, undergoes dimerization in acetone yielding the hydroxido–bridged $[\{V^VO(L^2)\}_2\mu–(HO)_2]$ **5**, having distorted octahedral geometry around each vanadium. In contrast, from a solution of **4** in acetonitrile, the dinuclear compound $[\{V^VO(L^2)\}_2\mu–O]$ **6** is obtained, with trigonal bipyramidal geometry around each vanadium. The methoxido complex **2** is successfully employed as a functional catechol–oxidase mimic in the oxidation of catechol to *o*–quinone under air. The process is confirmed to follow a Michaelis–Menten type kinetics with respect to catechol, the V_{max} and K_M values obtained being 7.66×10^{-6} M min^{-1} and 0.0557 M, respectively, and the turnover frequency is 0.0541 min^{-1}. The similar reaction with the bulkier 3,5–di–*tert*–butylcatechol proceeds at much slower rate. Complex **2** is also used as a catalyst precursor for the oxidative bromination of thymol in aqueous medium. The selectivity shows quite interesting trends, namely when not using excess of

primary oxidizing agent, H_2O_2: the *para* mono–brominated product corresponds to ~93 % of the products and no dibromo derivative is formed.

_____

† Electronic supplementary information (ESI) available: Details of [51]V NMR and other spectral studies. CCDC 1413240-1413244. For ESI and crystallographic data in CIF or other electronic format see DOI: $$$$$.

Introduction

The understanding of the role of vanadium in biological systems and its possible use in therapeutics has gathered increasing attention over the recent years. One of the most explored areas is the role of vanadium in decreasing blood glucose levels, where vanadium compounds are known to mimic most of the actions of insulin by inhibiting protein tyrosine phosphatases (PTPs).[1] Additionally, several vanadium compounds have also been successfully tested for their antitrypanosomal, antileishmanial, antiamoebic and DNA binding activities.[1(a), 2]

On the other hand, a similarly relevant field of interest in vanadium chemistry is based on the catalytic potential of vanadium compounds, namely for oxidation, oxidative halogenations and sulfoxidations of a variety of organic substrates.[3] Haloperoxidases are peroxidases that are able to catalyse the oxidation of halides by hydrogen peroxide, thereby achieving the halogenation of organic substrates.[1(f),4] Several structural and functional models of vanadium haloperoxidases (VHPOs) have been prepared and tested, and most of these compounds contain $V^{IV}O/V^VO$ and/or V^VO_2 units coordinated to O,N,O/S donor ligands. Recently vanadium compounds, predominantly with tripodal ligands, have also been employed in the catalysis of olefin polymerization. These vanadium catalysts display excellent thermal stability and generate high molecular mass poly–olefins with narrow range of molecular mass distribution.[5] Such types of V^V–complexes with tetradentate tripodal ligands exhibit interesting structural and solution phase properties.[6] They have also been applied for several catalytic oxidations.[7,8] In contrast, reports on vanadium based catechol oxidase mimics have seldom appeared.[9]

Catechol oxidase is an enzyme that catalyses the oxidation of phenols such as catechol. It is a copper–containing enzyme whose activity is similar to that of tyrosinase, a related class of copper oxidases. The enzyme contains the so–called type–3 Cu binding site, where dopa (3-hydroxy-L-tyrosine) is oxidized to dopa quinone coupled with $2e/2H^+$ reduction of O_2 to H_2O. The generated dopa quinone is further oxidized, in a four electron

process, to indolquinone. Indolquinone undergoes auto–polymerization producing a brown polyphenolic pigment, i.e., melanin, a process which is considered to protect damaged tissues against pathogens or insects.[10] The active site contains the $\{Cu(His)_3\}_2\mu$-O core, where two of the Cu^{II}–centers are coordinated to three histidine N–atoms and bridged by an external hydroxide moiety in a trigonal pyramidal geometry.[11-13] Several Cu based models have been prepared and studied for the establishment of structure/activity relationships.[14] Notwithstanding, there are numerous reports in literature where functional models with Co(II/III), Mn(III/II), Fe(III), Ni(II), Zn(II) centers, instead of Cu(II), have been used to achieve moderate to excellent conversion of catechol to o–quinone.[15]

Ramadan *et al.* reported a series of $V^{IV}O$–picolyl hydrazones as functional catechol oxidase models in the presence of a base at room temperature.[9] Similar results, but at elevated temperature, were reported by Hu *et al.* by using a V–polyoxidometalate.[16] In another report $Gd^{III}/V^{IV}O$ cryptate was used to mimic catechol oxidase action.[17] However, to the best of our knowledge, there have been no reports of V^{V}–complexes acting as catechol oxidase functional mimics. Recently some of us reported a polymer supported vanadium based polyphenol oxidase mimicking system for the oxidation of pyrogallol.[18] Herein, we report the synthesis and characterization of oxido/oxidomethoxido V^{V}–compounds, based on a tripodal ligand derived from aminoethylpyridine, formaldehyde and 2,4–di–*tert*–butylphenol using a modified Mannich condensation. Our attempts towards isolation of V^{IV}–complexes led to the hydrolysis of the tripodal amine, leaving an O,N,O donor tridentate amine coordinated to a V^{V}–centre. Some of these complexes mimic the action of catechol oxidase at room temperature, oxidising catechol to its quinone, without the use of base.

Experimental Section

Materials and general methods

V_2O_5 (Loba Chem, India), 2–aminoethylpyridine (Sigma Aldrich, USA), acetyl acetone (SRL, India), formaldehyde (Rankem, India), 2,4–di–*tert*–butylphenol (Himedia, India), 30% aqueous H_2O_2 (Qualigens, India), catechol (SDFCL, India), thymol (SDFCL, India) were used as obtained. Other chemicals and solvents were of AR grade. The precursor complex $[V^{IV}O(acac)_2]$ was prepared following a reported method.[19]

Elemental analyses of the complexes were carried out on an Elementar model Vario–EI–III after drying the samples at 100 ˚C. IR spectra were recorded as KBr pellets on a Nicolet 1100 FT–IR spectrometer. Electronic spectra of complexes were recorded in chloroform or

dichloromethane on a Shimadzu 1601 UV–Vis spectrophotometer. ^{1}H NMR and ^{13}C NMR spectra were recorded in $CDCl_3$ on a Bruker Avance 500 MHz spectrometer. The [51]V NMR spectra were obtained either on Bruker Avance+ 400 MHz or 300 MHz Spectrometers. The [51]V chemical shifts (δ_V) are expressed in ppm relative to neat V^VOCl_3, used as an external reference sample. High resolution mass spectra (HRMS) in positive ion electrospray ionization mass spectrometry mode were obtained on a Bruker micrOTOF–Q II mass spectrometer in CH_3CN. The electron paramagnetic resonance (EPR) spectra were measured with a Bruker ESP 300E X-band spectrometer, in frozen samples at 77 K, using DPPH radical as reference. The measured spectra (1st derivative X-band EPR) were simulated with the computer program developed by Rockenbauer and Korecz.[20]

X–Ray crystal structure determinations

Three–dimensional X–ray data were collected on a Bruker Kappa Apex CCD diffractometer at low temperature for **1**, **2**, **5** and **6** and at room temperature for **3**, by the ϕ–ω scan method. Reflections were measured from a hemisphere of data collected from frames, each of them covering 0.3º in ω. 132448 for **1**, 96907 for **2**, 76068 for **3**, 48486 for **5** and 22722 for **6** reflections measured were corrected for Lorentz and polarization effects and for absorption by multi–scan methods based on symmetry–equivalent and repeated reflections. Of them, 6289 for **1**, 7353 for **2**, 6272 for **3**, 3839 for **5** and 3408 for **6**, independent reflections exceeded the significance level ($|F|/\sigma|F|$) > 4.0, respectively. After data collection, in each case an empirical absorption correction (SADABS) was applied, and the structures were solved by direct methods and refined by full matrix least–squares on F^2 data using SHELX suite of programs.[21,22] In **1** and in **3**, hydrogen atoms were included in calculated position and refined in the riding mode. In **2**, hydrogen atoms were included in calculated positions and refined in the riding mode, except for O(2M), O(3M), C(3), C(5), C(10), C(12), C(18), C(19), C(20) and C(21), which were located in the difference Fourier map and left to refine freely. In **5**, hydrogen atoms were included in calculated positions and refined in the riding mode, except for N(1), which was located in the difference Fourier map and left to refine freely, and for O(1), which was located in the difference Fourier map and then fixed to the oxygen atom. In **6**, H–atoms were included in calculated positions and refined in the riding mode, except for N(1), C(3), C(5), C(18) and C(20), which were located in the difference Fourier map and left to refine freely. Refinements were done with allowance for thermal anisotropy of all non–hydrogen atoms. Final difference Fourier maps showed no residual density outside: 2.200

and –0.537 e.Å^{-3} for **1**, 0.567 and –0.732 for **2**, 0.498 and -0.461 for **3**, 0.539 and –0.674 for **5** and 0.913 and –0.769 e.Å^{-3} for **6**. A weighting scheme $w = 1/[\sigma^2(F_o^2) + (0.082900\ P)^2 + 50.612396\ P]$ for **1**, $w = 1/[\sigma^2(F_o^2) + (0.094900\ P)^2 + 0.702300\ P]$ for **2**, $w = 1/[\sigma^2(F_o^2) + (0.126300\ P)^2 + 0.000000\ P]$ for **3**, $w = 1/[\sigma^2(F_o^2) + (0.065900\ P)^2 + 1.096700\ P]$ for **5** and $w = 1/[\sigma^2(F_o^2) + (0.124900\ P)^2 + 0.000000\ P]$ for **6**, where $P = (|F_o|^2 + 2|F_c|^2)/3$, were used in the latter stages of refinement. The crystal of **1** presents a high residual electron density next to O(1), which has not been possible to refine. An important disorder on *t*–butyl groups appear in the crystal of **3**. These disorders were refined and two atomic sites have been observed and refined with the anisotropic atomic displacement parameters for three *t*–butyl groups. More specifically these disorders were refined using 274 restraints (SADI, SIMU, DELU and DFIX restraints were used). The site occupancy factors were 0.56667 for C(27A)–C(28A)–C(29A), 0.44182 for C(31A)–C(32A)–C(33A) and 0.83216 for C(60A)–C(61A)–C(62A). Other disorders appear around C(6) and C(43) atoms in the ligand, which were refined and two atomic sites were observed and refined with the anisotropic displacement parameters for the two atoms. These disorders were refined using 82 restraints (SADI, SIMU and DELU restraints were used). The site occupancy factors were 0.84836 for C(6A) and 0.74491 for C(43A). A disordered acetone molecule is present in the crystal packing of **5**. More specifically this disorder was refined using 79 restraints (SADI, SIMU and DELU restraints were used). The site occupancy factor was 0.41198 for C(1SA)–C(2SA)–O(1SA). Further details of the crystal structure determinations are given in Table 1.

Table 1 Crystal Data and Structure Refinement for $[V^VO(acac)(L^1)]\cdot0.5CH_3CN$ **1**, for $[V^VO(OMe)(MeOH)(L^1)]\cdot MeOH$ **2**, $[\{V^VO(L^1)\}_2\mu–O]$ **3**, $[\{V^{(IV)}O(L^2)\}_2\mu(OH)_2]\cdot2(CH_3)_2CO$ **5** and $[\{V^{(V)}O(L^2)\}_2\mu–O]$ **6**.

	$1\cdot0.5CH_3CN$	$2\cdot MeOH$	3	$5\cdot2(CH_3)_2CO$	6
Formula	$C_{43}H_{60.5}\ N_{2.5}\ O_5\ V$	$C_{40}\ H_{63}\ N_2\ O_6\ V$	$C_{74}\ H_{104}\ N_4\ O_7\ V_2$	$C_{66}\ H_{104}\ N_2\ O_{10}\ V_2$	$C_{60}\ H_{90}\ N_2\ O_7\ V_2$
Formula weight	743.38	718.86	1263.49	1187.39	1053.22
T, K	100(2)	100(2)	293(2)	100(2)	100(2)
Wavelength, Å	0.71073	0.71073	0.71073	0.71073	0.71073
Crystal system	Monoclinic	Triclinic	Triclinic	Monoclinic	Orthorhombic
Space group	$P2_1/n$	$P\ \bar{1}$	$P\ \bar{1}$	$P2_1/c$	Pbcn
a/Å	15.7992(10)	7.9065(5)	10.6149(6)	9.7921(19)	24.9968(16)
b/Å	13.8716(8)	14.5215(9)	15.8957(9)	28.523(6)	11.8900(8)
c/Å	19.3649(12)	19.1809(12)	23.0172(12)	11.769(3)	19.5013(15)
α/°		67.981(3)	80.123(3)		
β/°	91.760(2)	82.406(4)	85.922(3)	93.467(15)	
γ/°		86.889(3)	75.312(3)		
V/Å^3	4242.0(4)	2023.7(2)	3699.6(4)	3280.9(12)	5796.0(7)
Z	4	2	2	2	4
F_{000}	1596	776	1356	1280	2264
D_{calc}/g cm^{-3}	1.164	1.180	1.134	1.202	1.207
μ/mm^{-1}	0.278	0.290	0.304	0.341	0.374
θ/ (°)	1.69 to 26.46	1.15 to 27.81	0.90 to 28.06	2.08 to 29.25	1.63 to 25.51
R_{int}	0.1098	0.0672	0.1012	0.1841	0.1019
Crystal size/ mm^3	$0.30 \times 0.23 \times 0.07$	$0.47\times 0.36 \times 0.32$	$0.29 \times 0.21 \times 0.16$	$0.25 \times 0.13 \times 0.05$	$0.35 \times 0.21 \times 0.19$
Goodness–of–fit on F^2	1.156	1.041	0.943	1.025	1.055
$R_1[I>2\sigma(I)]$ [a]	0.1032	0.0502	0.0771	0.0753	0.0851
wR_2 (all data) [b]	0.3247	0.1573	0.2632	0.2032	0.2319
Largest differences peak and hole (eÅ^{-3})	2.200 and -0.537	0.567 and –0.732	0.498 and -0.461	0.539 and -0.674	0.913 and –0.769

$^a R_1 = \Sigma\,||F_o|-|F_c||\,/\Sigma\,|F_o|$. $^b wR_2 = \{\Sigma[w(||F_o|^2-|F_c|^2|)^2]|/\Sigma[w(F_o^2)^2]\}^{1/2}$

Synthetic procedures

6,6'–(2–(pyridin–2–yl)ethylazanediyl)bis(methylene)bis(2,4–di–*tert*–butylphenol),   H₂L¹

I. The compound was prepared following a literature method with slight modifications.[23] A solution of 2–aminoethylpyridine (2.440 g, 20.0 mmol), formaldehyde 30% (3.076 g, 40.0 mmol) and 2,4–di–*tert*–butylphenol (8.254 g, 40.0 mmol) was refluxed in MeOH (30.0 mL) for 12 h. Upon cooling to room temperature, a white solid precipitated out, which was filtered, washed with MeOH and dried in vacuum. Yield: 5.281 g (47%). (Found: C, 79.93; H, 9.47; N, 5.03; $C_{37}H_{54}N_2O_2$ (558.84 g mol⁻¹) requires, C, 79.52; H, 9.74; N, 5.01).

[V^{V}O(acac)(L¹)]   1. A solution of [V^{IV}O(acac)₂] (0.265 g, 1.0 mmol) in acetonitrile (10.0 mL) was added to a solution of **I** (0.559 g, 1.0 mmol) in hot acetonitrile (30.0 mL). The resulting solution was refluxed in a water bath for 8 h, affording a dark blue solution. After reducing the solvent volume to *ca.* 15 mL and cooling to room temperature, a black crystalline product slowly separated. It was filtered, washed with cold MeCN and dried in a vacuum desiccator over silica gel. Crystals of **1**·0.5CH₃CN suitable for X–ray diffraction (XRD) analysis were grown by slow evaporation of an acetonitrile solution at 4 °C in a refrigerator. Yield: 0.585 g (81%). (Found: C, 69.50; H, 7.94; N, 3.58; $C_{42}H_{59}N_2O_5V$ (722.87 g mol⁻¹) requires, C, 69.78; H, 8.23; N, 3.88). IR υ_{max}/ cm⁻¹: 2957, 2906, 2866, 1584, 1525, 1470, 1436, 1360, 1246, 1170, 959 (V=O), 853, 759, 580, 481. ¹H NMR (CDCl₃)/ δ: 8.44–8.42 (d, 1H, Py), 7.51–7.47 (m, 1H, Ar), 7.31–7.30 (d, 2H, Ar), 7.06–7.05 (m, 3H, Ar), 6.87–6.85 (d, 1H, Ar), 5.60 (s, 1H, –CH=), 3.44–3.41 (d, 2H, NCH₂Ar), 2.92 (s, 2H, NCH₂Ar), 2–2.05 (d, 2H, NCH₂CH₂), 2.25(s, 2H, NCH₂CH₂), 1.93 (s, 6H, –CH₃), 1.31(s, 18H, C(CH₃)₃) 1.57(s, 18H, –C(CH₃)₃).

[V^{V}O(OMe)(MeOH)(L¹)] 2. A solution of [V^{V}O(acac)(L¹)] **1** (0.723 g, 1.0 mmol) in MeOH (40.0 mL) was heated under reflux for 3 days with stirring. The resulting solution was cooled and kept in air for slow precipitation of the black crystalline compound. It was filtered, washed with cold MeOH and dried in a vacuum desiccator over silica gel. Crystals of **2**·MeOH suitable for X–ray diffraction analysis were grown by slow evaporation of its MeOH solution. Yield: 0.515 g (75%). (Found: C, 68.50; H, 8.85; N, 4.15; $C_{39}H_{59}N_2O_5V$ (686.84 g mol⁻¹) requires, C, 68.20; H, 8.66; N, 4.08). IR υ_{max}/ cm⁻¹: 3412, 2954, 2903, 2867, 1474, 1442, 1361, 1236, 1204, 1169, 1049, 1024 (V=O), 1008, 843, 756, 621, 598, 559.

[{V^{V}O(L¹)}₂μ–O] 3. Method A: A solution of [V^{V}O(OMe)(MeOH)(L¹)] **2** (0.687 g, 1.0 mmol) in acetone (40.0 mL) or MeCN was heated under reflux for 24 h. The resulting solution was cooled at 4 ºC for ca. 2 days from where the black complex **3** slowly

precipitated out. It was filtered, washed with cold acetone and dried in vacuum. Yield: 0.482 g (74%). (Found: C, 69.88; H, 8.0; N, 4.43; $C_{74}H_{104}N_4O_7V_2$ (1263.52 g mol^{-1}) requires, C, 70.34; H, 8.30; N, 4.43). IR υ_{max}/ cm^{-1}: 2954, 2903, 2866 (*tert*-butyl), 1467, 1441, 1361, 1279, 1238, 1170, 936 (V=O), 855 (V–μ–O–V) 758, 689, 668, 569, 476. ^{1}H NMR (CDCl$_3$)/ δ: 9.83 (s, 2H Py), 7.36–7.33 (t, 2H, Ar), 7.02–6.99 (t, 2H, Ar), 6.96 (s 4H, Ar), 6.86 (s, 4H, Ar) 6.70–6.68 (d, 2H, Ar), 6.03–6.00 (d, 4H, NCH$_2$Ar), 3.24–3.21 (d, 4H, NCH$_2$Ar), 2.80 (s, 4H, NCH$_2$CH$_2$), 2.51 (s, 4H, NCH$_2$CH$_2$), 0.86 (s, 36H, –C(CH$_3$)$_3$), 1.24 (s, 36H, –C(CH$_3$)$_3$).

Method B: Slow evaporation of a filtered acetonitrile solution of [V^{V}O(acac)(L^1)] **1** at room temperature produced dark green crystals of **3** in poor yields in ca. 3 days.

H[V^{V}O$_2$(L^2)] 4. A solution of H$_2$L^1 (0.558 g, 1.0 mmol) in 20.0 mL ethanol was added to a solution of VOSO$_4$·5H$_2$O (0.253 g 1.0 mmol) in aqueous–ethanol (1:4, 5.0 mL). The resulting solution was refluxed for 8 h to obtain a dark brown solution. After reducing the solution volume to ca. 10 mL and keeping at room temperature, a dark brown solid slowly precipitated. It was filtered, washed with cold ethanol and dried in vacuum. Attempts to obtain adequate crystals of this compound were not successful. Yield: 0.274 g (51%). (Found: C, 67.24; H, 8.14; N, 2.60; C$_{30}$H$_{44}$NO$_4$V (535.63 g mol^{-1}) requires, C, 67.27; H, 8.66; N, 2.61). No satisfactory ^{1}H or ^{51}V NMR could be obtained for this compound. The samples had a very weak EPR signal, due to the presence of a small amount of a V^{IV}-species, probably an impurity (see below). IR υ_{max}/ cm^{-1} (see Fig. S1): 3448 (OH), 3181 (NH), 2955, 2913, 2867 (*tert*-butyl), 1467, 1440, 1357, 1239, 1168, 1130, 1047, 994, 969 (VO$_2$), 872, 854, 759, 645, 596.

[{V^{V}O(L^2)}$_2$μ(OH)$_2$] 5. Method A: A solution of **4** (0.200 g, 0.37 mmol) in acetone (40.0 mL) was heated under reflux for 3 h. The resulting solution was cooled at 4 °C for 2 days, where black crystals of **5**·2(CH$_3$)$_2$CO were slowly formed. The solid was filtered, washed with cold acetone, and dried in a vacuum desiccator over silica gel. Yield: 0.187 g (89%). (Found: C, 67.06; H, 8.63; N, 2.43; C$_{60}$H$_{92}$N$_2$O$_8$V$_2$ (1071.26 g mol^{-1}) requires, C, 67.27; H, 8.66; N, 2.61). For X–ray diffraction single crystals of **5**·2(CH$_3$)$_2$CO were used as such. IR υ_{max}/ cm^{-1} (see Fig. S2): 3568, 3433, 3259, 2955, 2904, 2866, 1458, 1362, 1239, 1203, 1171, 957 (V=O), 870 (V–μ–O–V), 777, 756, 603, 586. ^{1}H NMR (CDCl$_3$)/ δ: 7.31 (s, 1H, Ar), 7.27 (s, 2H, Ar), 7.05 (s, 4H, Ar), 7.00 (s, 1H, Ar), 4.01–3.98 (d, 3H, NCH$_2$Ar), 3.47–3.42 (t, 3H, NCH$_2$Ar), 3.23 (s, 1H, NCH$_2$Ar), 3.06 (s, 1H, NCH$_2$Ar), 1.41–1.42 (d, 36 H, –C(CH$_3$)$_3$), 1.28–1.31 (d, 36H, –C(CH$_3$)$_3$), 4.20 (br s, 1H, NH), 4.13 (br s, 1H, NH).

Method B: A solution of H_2L^1 (0.558 g, 1.0 mmol) in acetonitrile (20.0 mL) was added to a solution of $V^{IV}OSO_4 \cdot 5H_2O$ (0.253 g, 1.0 mmol) in aqueous:acetonitrile (1:4, 5.0 mL). The resulting solution was refluxed for 8 h to obtain a dark coloured solution. It was neutralized by drop wise addition of 1 equivalent of sodium hydroxide, whereupon a black solid precipitated. It was filtered, washed with cold acetone and dried in a vacuum desiccator over silica gel. Yield: 63%.

$[\{V^VO(L^2)\}_2\mu-O]$ 6. A solution of **4** (0.100 g, 0.19 mmol) in MeCN (40.0 mL) was heated under reflux for 18 h. The resulting solution was maintained at 4 ˚C for ca. 2 days, from where black crystals were obtained. The product was filtered, washed with cold acetonitrile and dried in a vacuum desiccator over silica gel. Yield: 0.075 g (74%). (Found: C, 67.50; H, 8.18; N, 2.84; $C_{60}H_{90}N_2O_7V_2$ (1053.56 gmol^{-1}), including ½ H_2O requires, 67.84; H, 8.63; N, 2.64). For X–ray diffraction single crystals of **6** were used as such. IR υ_{max}/ cm^{-1} (see Fig. S3): 3261, 2959, 2905, 2866, 1465, 1437, 1362, 1235, 1170, 1127, 1002 (V=O), 839 (V–μ–O–V), 764, 723, 702, 601, 572, 540. ^1H NMR (CDCl$_3$)/ δ: 7.28 (s, 4H, Ar), 7.05 (s, 2H, Ar), 7.00 (s, 2H, Ar), 4.00–3.98 (d, 4H, NCH$_2$Ar), 3.47–3.42 (m, 2H, NCH$_2$Ar), 3.21(s, 1H, NCH$_2$Ar), 2.97 (s, 1H, NCH$_2$Ar), 1.41–1.43 (d, 36H, –C(CH$_3$)$_3$), 1.31–1.32 (d, 36H, –C(CH$_3$)$_3$), 4.58 (br s, 1H, NH), 4.19 (br s, 1 H, NH).

Catechol Oxidase Mimetic Activity

The oxidomethoxido complex **2** was chosen as representative to study the catalytic oxidation of catechol. The reaction was carried out in normal methanol and was studied by monitoring the increase in absorbance at 383 nm due to *o*–benzoquinone formation using a UV–visible spectrophotometer for a period of 1 h. Two sets of reactions were carried out: one in atmospheric air and the other in an atmosphere of molecular oxygen. The reaction was initiated with the addition of a 5.0 mL solution of $[V^VO(OMe)(MeOH)(L^1)]$ (3.9834×10^{-4} M) in methanol to 10.0 mL of a solution of catechol (1.00×10^{-1} M). The steady state kinetic experiments were carried out by varying the catechol concentration (0.0250–0.1750 M) in the presence of $[V^VO(OMe)(MeOH)(L^1)]$ (3.9834×10^{-4} M). The reaction was studied by mixing 1.0 mL of the solution containing the catalyst in methanol to 2.0 mL of catechol solution in methanol, and monitoring the increase of absorbance at 383 nm (ε = 1900 M^{-1} cm^{-1} for 3,5–di–*tert*–butyl quinone)[11] as a function of time on a UV–Vis spectrophotometer after 3 minutes of preparation. The initial rates were calculated from the slope of the plot of absorbance versus time, over a period of 3 minutes. The initial reaction rates were then fitted to the Michaelis–Menten equation and Lineweaver Burk plot to calculate the parameters:

maximal velocity (V_{max}), Michaelis constant (K_M) and catalytic constant or turnover number (k_{cat}) from nonlinear curve fit using Origin 8.0 software.

Vanadium haloperoxidase activity: catalytic oxidative bromination of thymol

The oxidomethoxido complex **2** was used to catalyse the oxidative bromination of thymol in aqueous medium. In a typical reaction, thymol (1.500 g, 10.0 mmol), KBr (2.380 g, 20.0 mmol), H_2O_2 (2.267 g, 20.0 mmol) and water (20.0 mL) were taken in a 50 mL reaction flask. The catalyst (0.0010 g) and $HClO_4$ (0.717 g, 0.50 mmol) were added and the mixture was stirred at room temperature. An additional 1.50 mmol of $HClO_4$ was added in three equal portions at intervals of fifteen minutes. After 2 h the reaction mixture was extracted with dichloromethane, washed with brine (NaCl) solution and dried over anhydrous Na_2SO_4. The reaction products were separated using a silica gel column. The products were analysed and identified by GC, GC–MS and ^{1}H NMR.

Results and Discussion

The reaction of the ligand H_2L^1 **I** with one equivalent of $[V^{IV}O(acac)_2]$ in acetonitrile under ambient conditions gave dark blue crystals of $[V^VO(acac)(L^1)]$ **1** where the ligand acts as ONO tridentate coordinating through N–imine and O–phenolate atoms in a *cis* fashion (vide infra). The V^{IV}–center is oxidised to V^V during the process. A hot MeCN solution of **1**, upon cooling to 0 ˚C, yielded dark blue crystals of **1**, while a suspension of **1** in MeCN at room temperature slowly turned dark green in ca. 3 days and resulted in green crystals of an oxido bridged dinuclear complex $[\{V^VO(L^1)\}_2\mu–O]$ **3**. Upon prolonged treatment of **1** with MeOH the coordinated acac$^-$ is removed and the corresponding methoxido complex, $[V^VO(OMe)(MeOH)(L^1)]$ **2**, was isolated. This methoxido compound yielded **3** upon refluxing in MeCN or acetone. Attempts made to isolate the V^{IV}–complex of H_2L^1 by the reaction of ligand with $V^{IV}OSO_4$ in ethanol resulted in the formation of $H[V^VO_2(L^2)]$ **4** (where H_2L^2 **II** is the tridentate ligand obtained upon loss of the ethylpyridine fragment of **I**). The proton may either be protonating an O-phenolate, or the N-amine atom (or even the O-oxido atom). The elemental analysis of **4** does not differ much from those of **5** and **6**, but the IR spectrum depicts some significant differences (Figs. S1 to S3), namely the absence of the strong sharp bands at 702 and 723 cm^{-1}, present in **6**. In **5** strong sharp bands are detected at 958 and 870 cm^{-1}, while in **4** sharp bands are observed at 994, 969 and 872 cm^{-1} (medium intensity), as well as a sharp band at 854 cm^{-1}. What we designate by **4** probably is not a pure compound and thus we cannot consider it as fully characterized.

Compound **4** in acetone gave black crystals of $[\{V^VO(L^2)\}_2\mu-(OH)_2]\cdot2(CH_3)_2CO$ **5**. The effect of solvent is yet again noticeable: while the reaction of **I** with $V^{IV}OSO_4.5H_2O$ in ethanol gave **4** as the only product, the same reaction in MeCN followed by base neutralization directly yielded the dinuclear species **5** as the major product. Moreover, a solution of **4** in acetonitrile resulted in the formation of the oxido bridged dinuclear compound $[\{V^VO(L^2)\}_2\mu-O]$ **6**.

The structural formulae of the compounds prepared are summarized in Scheme 1. All complexes are soluble in common organic solvents such as MeOH, EtOH, CH_2Cl_2, $CHCl_3$, acetone and acetonitrile. The presence of *tert*–butyl groups also allows solubility of these compounds in hydrocarbon–type solvents such as hexane and heptane.
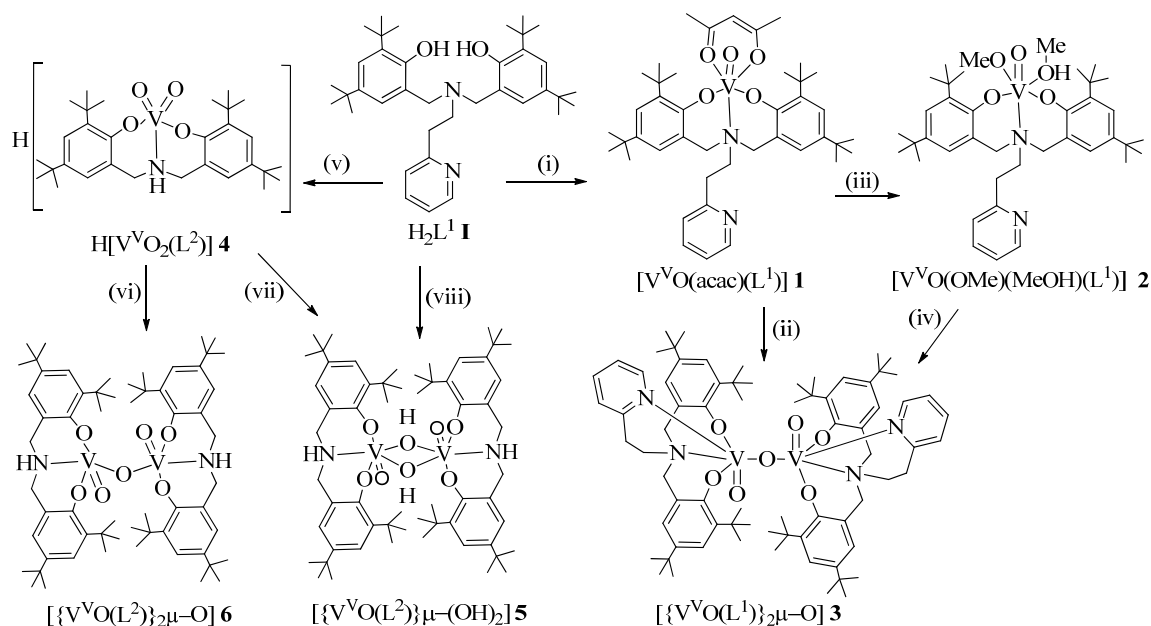
Scheme 1 Structural formulae and numbering of the compounds along with their synthetic routes. Conditions: (i) $[V^{IV}O(acac)_2]$/ MeCN, Δ; (ii) MeCN/ RT; (iii) MeOH, Δ; (iv) MeCN, Δ; (v) $V^{IV}OSO_4\cdot5H_2O$/ EtOH, Δ; (vi) MeCN; (vii) Acetone; (viii) $V^{IV}OSO_4\cdot5H_2O$/ MeCN, Δ. L^2 corresponds to the ONO tridentate ligand obtained upon elimination of the ethylpyridine moiety of H_2L^1.

Description of structure of the compounds

Compound $[V^VO(acac)(L^1)]\cdot 0.5CH_3CN$ **1** crystallized from acetonitrile as black crystals and Fig. 1 depicts an ORTEP representation. The asymmetric unit of **1** contains one mononuclear complex and half acetonitrile molecule. Compound $[V^VO(OMe)(MeOH)(L^1)]\cdot MeOH$ **2** crystallized from methanolic solution as black crystals and Fig. 2 presents an ORTEP representation. In **2** the asymmetric unit contains one mononuclear complex and one methanol molecule. Compound **3**, $[\{V^VO(L^1)\}_2\mu–O]$, crystallized from acetonitrile solution and the asymmetric unit contains two half's of two dinuclear complexes (see Fig. 3). In the dinuclear compound **5**, $[\{V^VO(L^2)\}_2\mu–(OH)_2]\cdot 2(CH_3)_2CO$, the ligand that binds to each vanadium, L^2, corresponds to L^1 after the elimination of the aminoethylpyridine group; it crystallized from acetone as black crystals. Fig. 4 shows the dinuclear compound, and the asymmetric unit contains half dinuclear complex and one acetone molecule. In compound $[\{V^VO(L^2)\}_2\mu–O]$ **6** the ligand is the same as in **5** and the asymmetric unit only contains half complex; Fig. 5 depicts a representation of this compound. Table 2 provides selected bond lengths and bond angles for compounds **1**, **2**, **3**, **5** and **6**.

Table 2 Bond Lengths [Å] and Angles [°] for $[V^VO(acac)(L^1)]\cdot 0.5CH_3CN$ **1**, $[V^VO(OMe)(MeOH)(L^1)]\cdot MeOH$ **2**, $[\{V^VO(L^1)\}_2\mu–O]$ **3**, $[\{V^VO(L^2)\}_2\mu(OH)_2]\cdot 2(CH_3)_2CO$ **5** and $[\{V^VO(L^2)\}_2\mu–O]$ **6**.

Bond lengths	1	2	3	5	6
V(1)-O(1)	1.594(4)	1.5884(14)	1.843(3)	1.965(3)	1.832(3)
V(1)-O(2)	1.839(4)	1.8455(14)	1.856(3)	1.836(3)	1.859(3)
V(1)-O(3)	1.817(4)	1.8548(14)	1.606(3)	1.600(3)	1.583(3)
V(1)-O(4)	1.989(4)		1.7932(8)	1.844(3)	1.7896(9)
V(1)-O(5)	2.008(5)				
V(1)-O(1)#1				1.991(3)	
V(1)-O(1M)		1.8187(14)			
V(1)-O(2M)		2.2834(15)			
V(1)-N(1)	2.452(5)	2.3472(16)	2.395(3)	2.350(4)	2.149(4)
V(1)-N(2)			2.328(4)		
V(2)-O(5)			1.851(3)		
V(2)-O(6)			1.843(3)		
V(2)-O(7)			1.603(3)		
V(2)-O(8)			1.7941(7)		
V(2)-N(3)			2.386(3)		
V(2)-N(4)			2.337(4)		
Angles	1	2	3	5	6
O(1)–V(1)–O(3)	98.5(2)	100.28(7)	96.34(14)	97.13(13)	109.46(15)

O(1)–V(1)–O(2)	100.6(2)	100.04(7)	161.36(13)	93.85(12)	140.34(13)
O(3)–V(1)–O(2)	99.2(2)	154.98(6)	96.48(14)	97.47(13)	105.25(15)
O(1)–V(1)–O(4)	96.3(2)		95.59(10)	157.28(12)	92.66(10)
O(3)–V(1)–O(4)	88.66(18)		100.97(12)	98.65(13)	107.06(16)
O(2)–V(1)–O(4)	160.01(19)		95.19(11)	100.17(13)	95.03(14)
O(1)–V(1)–O(5)	94.2(2)				
O(3)–V(1)–O(5)	165.91(19)				
O(2)–V(1)–O(5)	84.54(19)				
O(4)–V(1)–O(5)	83.73(19)				
O(1)–V(1)–N(1)	176.2(2)	90.73(6)	82.24(12)	81.45(12)	81.31(14)
O(3)–V(1)–N(1)	82.05(18)	82.56(6)	170.83(15)	178.38(14)	93.84(15)
O(2)–V(1)–N(1)	82.96(18)	82.73(6)	82.94(12)	81.88(13)	77.77(13)
O(4)–V(1)–N(1)	79.93(17)		88.19(9)	82.94(12)	159.06(15)
O(5)–V(1)–N(1)	84.94(17)				
O(3)–V(1)–O(1)#1				98.20(13)	
O(2)–V(1)–O(1)#1				160.62(12)	
O(4)–V(1)–O(1)#1				88.68(12)	
O(1)–V(1)–O(1)#1				72.94(13)	
V(1)–O(4)–V(1)#2					
O(1)#1–V(1)–N(1)				82.14(12)	
V(1)–O(1)–V(1)#1				107.06(13)	
O(1)–V(1)–O(1M)		100.75(7)			
O(1M)–V(1)–O(2)		95.42(6)			
O(1M)–V(1)–O(3)		94.98(6)			
O(1)–V(1)–O(2M)		174.62(7)			
O(1M)–V(1)–O(2M)		84.63(6)			
O(2)–V(1)–O(2M)		79.53(6)			
O(3)–V(1)–O(2M)		78.87(6)			
O(1M)–V(1)–N(1)		168.51(6)			
O(2M)–V(1)–N(1)		83.89(6)			
O(3)–V(1)–N(2)			86.78(15)		
O(4)–V(1)–N(2)			172.26(10)		
O(1)–V(1)–N(2)			83.52(14)		
O(2)–V(1)–N(2)			83.75(15)		
N(2)–V(1)–N(1)			84.06(13)		
O(7)–V(2)–O(8)			101.94(11)		
O(7)–V(2)–O(6)			96.37(13)		
O(8)–V(2)–O(6)			96.73(9)		
O(7)–V(2)–O(5)			95.53(14)		
O(8)–V(2)–O(5)			95.01(10)		
O(6)–V(2)–O(5)			161.18(13)		
O(7)–V(2)–N(4)			86.39(15)		
O(8)–V(2)–N(4)			171.58(11)		
O(6)–V(2)–N(4)			83.38(14)		
O(5)–V(2)–N(4)			82.87(14)		
O(7)–V(2)–N(3)			169.87(13)		
O(8)–V(2)–N(3)			88.18(8)		
O(6)–V(2)–N(3)			82.35(12)		
O(5)–V(2)–N(3)			83.37(13)		
N(4)–V(2)–N(3)			83.49(13)		

14

Symmetry transformations used to generate equivalent atoms:

    #1 −x,−y,−z+1   #2 −x+2,y,−z+1/2
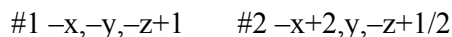
      The molecular structure of **1** consists on a six–coordinated mononuclear complex with a distorted octahedral geometry. The acac⁻ ligand normally binds strongly and the pyridine moiety does not participate in complex formation at least partly due to the oxophilicity of the V^V.[24] The axial sites of the octahedron are occupied by the oxido O–atom and by the bridgehead N–amine atom [V1–O1, 1.594(4) Å, V1–N1, 2.452(5) Å]. The remaining coordinating atoms approximately form a plane [O2–O3–O4–O5, mean deviation from plane, 0.0371(21) Å] and the V–atom is displaced toward the apical oxido ligand by 0.2502 Å. The two O–atoms from the acac⁻ ligand occupy two positions *cis* to V=O, a type of binding not commonly found in literature.[25,26] As expected the bond length to the amine N–atom *trans* to the oxido atom (V1–N1) is quite elongated, as a consequence of its *trans* influence.[27] The V–O_{ArO} bonds, which are *cis* to each other, have similar V–O distances (average 1.828(4) Å). The carbon–carbon and carbon–oxygen distances of the acac⁻ ligand do not allow to differentiate the ketonic oxygen from the enolic one, [O4–C39, 1.272(8) Å, O5–C41, 1.270(8) Å, C39–C40, 1.376(10) Å, C40–C41, 1.391(10) Å]. [25,26]
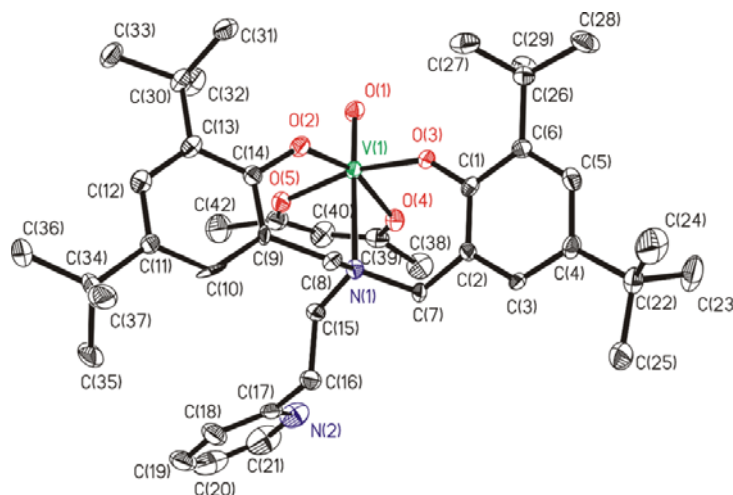
Fig. 1 ORTEP plot of the mononuclear V^V–complex in [V^VO(acac)(L¹)]·0.5CH₃CN **1**. All the non–hydrogen atoms are presented by their 50% probability ellipsoids. Hydrogen atoms are omitted for clarity.

The structure of **2** corresponds to a mononuclear complex with a six–coordinated distorted octahedral geometry. The axial sites of the octahedron are occupied by the oxido O–atom and by one methanol molecule [V1–O1, 1.5884(14) Å, V1–O2M, 2.2834(15) Å]. The other coordinated atoms form a plane [O2–O3–N1–O1M, mean deviation from plane, 0.0689(7) Å] with the vanadium atom displaced toward the apical oxido ligand by 0.2741 Å. The distances V1–O_{ArO} [V1–O2, 1.8455(14) Å and V1–O3, 1.8548(14) Å] are similar to V1–$O_{methoxido}$ [V1–O1M, 1.8187(14) Å]. As expected the bond length to the function *trans* to the oxido group (V1–O2M) is somewhat elongated, as a consequence of the *trans* influence,[27] but is shorter than in **1**. The methoxido and methanol molecules can easily occupy different positions and in **2** the V–O_{ArO} bonds are *trans* to each other. Intra and intermolecular hydrogen bonds exist between coordinated methoxido and coordinated and non–coordinated methanol molecules (see Table 3).
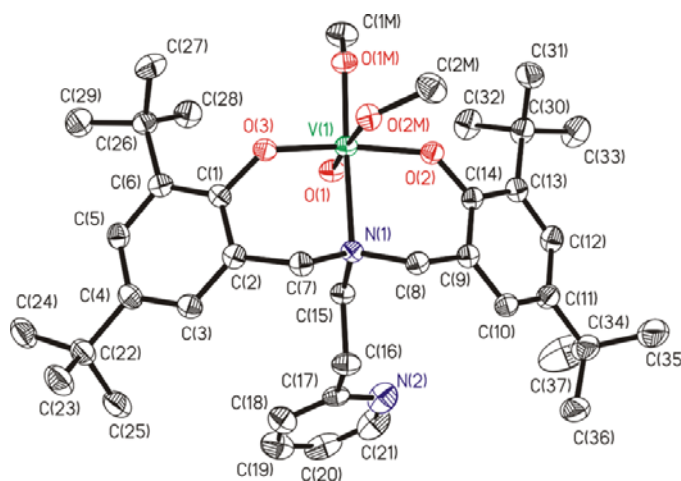
Fig. 2 ORTEP plot of the mononuclear V^V–complex in compound $[V^VO(OMe)(MeOH)(L^1)]\cdot MeOH$ **2**. All the non–hydrogen atoms are presented by their 50% probability ellipsoids. Hydrogen atoms are omitted for clarity.

The molecular structure of **3** consists of a dinuclear complex corresponding to a $[V_2O_3]^{4+}$ core with *anti*–linear configuration,[28] each V^V being bound to a tetradentate ONNO ligand (L^1) [Fig. 3 (a and b)]. The geometry around each vanadium centre is distorted octahedral with L^1 bound through the pyridine–N atoms [V1–N2, 2.328(4) Å and V2–N4, 2.338(4) Å], the bridgehead amine–N atoms (N_{amine}) [V1–N1, 2.328(4) Å and V2–N3, V2-N3, 2.386(3) Å], two phenolate–O atoms (O_{ArOe}) [V1–O1, 1.843(3) Å and V1–O2, 1.856(3)

Å, as well as V2–O5, 1.851(3) Å and V2–O6, 1.843(3) Å], one terminal O–atom [V1-O3, 1.606(3) Å and V2-O7, 1.603(3) Å] and one oxido bridge in each complex [V1-O4, 1.7932(8) Å and V2-O8, 1.7941(7) Å]. The V–atoms in each unit are displaced toward the apical oxido ligand from the equatorial plane defined by the two O_{ArO}, one N_{amine} and μ–oxo atoms by 0.1751 Å (in respect to the plane O1–O2–O3–N1, mean deviation from plane 0.0213(16) Å), and by 0.1909 Å (in respect to the plane O5–O6–O7–N3, mean deviation from plane 0.0214(14) Å). The two V=O bonds are very similar [average: 1.6015(30) Å] and characteristic of oxido–type O–atoms with strong π bonding. The V–μ–oxo bonds also depict some π–bonding character and have an average length of 1.7937(8) Å. The V–O_{ArO} bonds, which are trans to each other, are significantly shorter (average 1.848(3) Å) than the N–atoms that are *trans* to μ–oxo atoms or to V=O bond (average 2.362(3) Å) in a cis–α type structure.[29,30] The V–V separation is 3.587 Å in the two dinuclear units.[31]

(a)   (b)
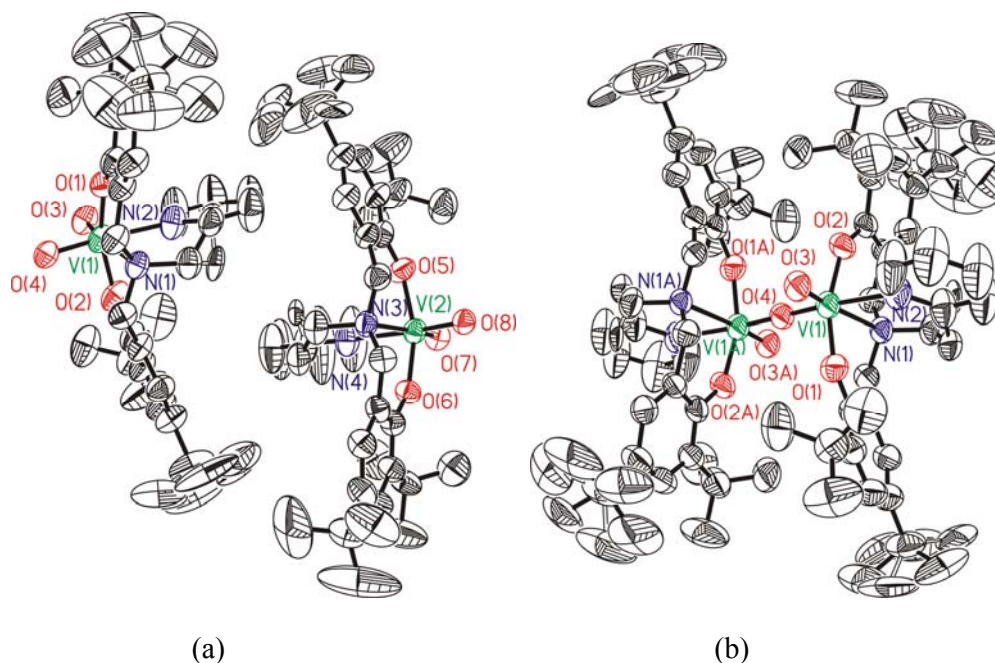
Fig. 3 ORTEP plot of $[\{V^VO(L^1)\}_2\mu–O]$ **3**. (a) Asymmetric unit showing two independent half molecules of **3**, and (b) the full dinuclear structure of **3**. All the non–hydrogen atoms are presented by their 30% probability ellipsoids. Hydrogen atoms are omitted for clarity.

Table 3 Hydrogen bonds for [$V^VO(OMe)(MeOH)(L^1)$]·MeOH **2** and [{$V^VO(L^2)$}$_2\mu$–(OH)$_2$]·2(CH$_3$)$_2$CO **5**.

D–H...A (compound)	d(D–H)	d(H...A)	d(D...A)	<(DHA)
O(2M)–H(2M)...O(3M)#1 **2**	0.90(3)	1.76(3)	2.650(2)	169(3)
O(3M)–H(3M)...O(1M) **2**	0.89(3)	1.89(3)	2.741(2)	160(3)
N(1)-H(1N)...O(3)#2 (**5**)	0.74(4)	2.48(4)	3.118(5)	145(4)

Symmetry transformations used to generate equivalent atoms:

#1 –x+1,–y+1,–z+1   #2 –x,–y,–z+1

In the molecular structure of **5** and **6** the complexes consist in dinuclear species containing two V^V–centers with ligand L^2, the difference being in the bridge between the V^V–atoms. In **5**, the bridge is formed by two OH groups, in an *anti*–orthogonal configuration. In **6,** the bridge is formed only by one O–oxido moiety in a *twist quasi–linear* configuration [V(1)–O(4)–V(1)#1, 166.6(3)º]. The V–centres adopt a distorted six–coordinated octahedral geometry in **5.** In **6**, the geometric parameter $\tau = (\beta - \alpha)/60$, where β and α are the two largest L–M–L angles, describes a coordination environment of five coordinated atoms; it has a value of 1 if the geometry is trigonal bipyramidal and 0 if it is square pyramidal.[32] For **6** ($\alpha_{O1-V1-O2}$ = 140.34º, $\beta_{O4-V1-N1}$ = 159.06º) the value of τ is 0.31, indicating a distorted square pyramidal geometry.[32,33] The ligand L^2 bound through the bridgehead amine–N atoms [V1–N1, 2.350(3) Å in **5** and 2.149(4) Å in **6**], two phenolic–O atoms [V1–O2, 1.836(3) Å in **5** and 1.859(3) Å in **6**, and V1–O4, 1.844(3) Å in **5** and 1.7896(9) Å in **6**] and terminal O–atoms [V1–O3, 1.600(3) Å in **5** and 1.583(3) Å in **6**]. In **5**, the vanadium atoms in each core are displaced toward the apical oxido ligand from the equatorial plane defined by the two O$_{ArO}$ atoms and two μ–hydroxide groups by 0.2600 Å (in respect to the plane O1–O2–O4–O1A, mean deviation from plane, 0.0022 Å). The V–V separation is 3.182 Å. In **6**, the axial position is occupied by an oxido–type O–atom with strong π bonding [V1–O3, 1.583(3) Å]. The basal positions are occupied by two O$_{ArO}$ atoms, one N$_{amine}$ atom and one oxido bridge, [V1–O1, V1–O2, V1–N1, V1–O4]. The torsion angle between the planes containing V1–O3 and V1A–O3A bonds (N1, O3, V1, O4 and N1A, O3A, V1A, O4) is 75.2º. The V–μ–oxido bonds also depict some π–bonding character [V1–O4, 1.7896(9) Å] and the V–V separation is 3.554 Å. Intermolecular hydrogen bonds exist between protonated N$_{amine}$ and oxido O–atoms of different complexes in **5**. (see Table 3).
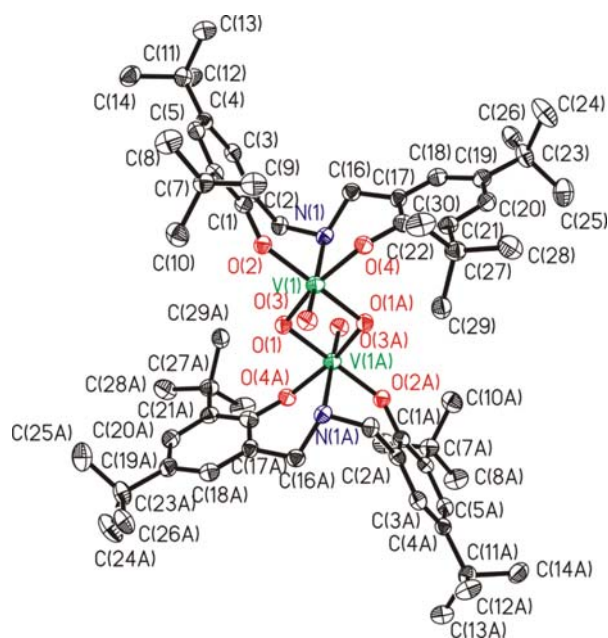
Fig. 4 ORTEP plot of $[\{V^{V}O(L^{2})\}_{2}\mu\text{–}(OH)_{2}]\cdot2(CH_{3})_{2}CO$ **5**. All the non–hydrogen atoms are presented by their 50% probability ellipsoids. Hydrogen atoms are omitted for clarity.
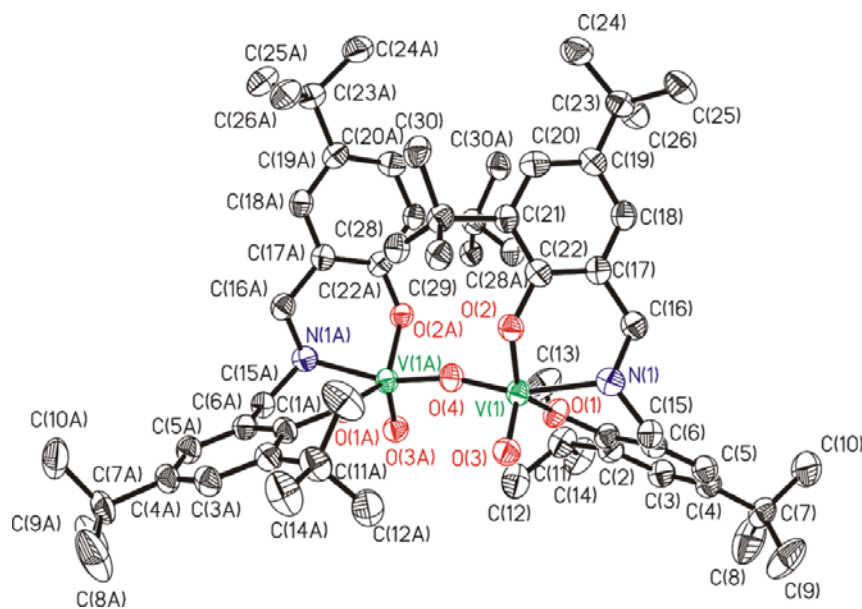
Fig. 5 ORTEP plot of $[\{V^{V}O(L^{2})\}_{2}\mu\text{–}O]$ **6**. All the non–hydrogen atoms are presented by their 50% probability ellipsoids. Hydrogen atoms are omitted for clarity.

IR Spectral Studies

A partial list of IR spectral data of the compounds is presented in Table 4 (For IR spectra of **4-6** see Figs. S1–S3). All V^{V}–complexes exhibit strong $v(V=O)$ bands in the range 936–1024

cm^{-1}. Dinuclear complexes **3**, **5** and **6** show one strong peak at 936–1002 cm^{-1} due to v(V=O) and another one arising at 853–880 cm^{-1}, probably due to the v(V–O–V) stretch.[34] In the spectrum of **5** a sharp peak appearing at 3567 cm^{-1} is probably due to the bridging OH group; the presence of single peak in the 936–1002 cm^{-1} region indicates the equivalence of the two bridged halves. The spectrum of complex **1** also displays the signature of carbonyl stretch at 1525 cm^{-1} due to the coordinated acac$^-$ moiety. The hydrolysis of the N–atom (acting like the tripodal) and the consequent presence of free NH is reflected by the sharp peak due to v(NH) stretch in complexes **4**, **5** and **6** at 3180–3261 cm^{-1}. The presence of two pairs of peaks at 969, 854 cm^{-1} and 992, 872 cm^{-1} in the spectrum of **4**, may be attributed to v_{asymm}(O=V=O) and v_{symm}(O=V=O) stretches in two distinct environments (e.g. two isomeric forms); some of these bands may also not be V=O stretches.

Table 4 Selected IR data for the compounds obtained with tentative assignments.

S.No.	Compounds	v(–OH)	v(V=O)	$v\left(V{\overset{O}{\diagup\diagdown}}V\right)$	v(N–H)
1.	[V^{V}O(acac)(L^1)] **1**		959		
2.	[V^{V}O(OMe)(MeOH)(L^1)] **2**	3400	1024 ^{a}		
3.	[{V^{V}O(L^1)}$_2$μ–O] **3**		936	855	
4.	H[V^{V}O$_2$(L^2)] **4**		969/994 872/854		3180
5.	[{V^{V}O(L^2)}$_2$μ–(OH)$_2$] **5**	3400	957	870	3259
6.	[{V^{V}O(L^2)}$_2$μ–O] **6**		1002	838	3261

^{a} There are a few weak IR bands in the region 930-915 cm^{-1}, and three medium/strong bands at 1008, 1049 and 1024 cm^{-1} (order of increasing intensity). In 2002, for C-[V^{IV}O(sal-L-Ala)(H$_2$O)], from a frequency calculation with the ADF-2000 program, the V=O stretching was calculated at 1028.7 cm^{-1}, while the experimental v(V=O) was found at 996 cm^{-1} (ref. 35), thus here we tentatively assign the v(V=O) to the and 1024 cm^{-1} band.

Electronic Spectral Studies

The electronic spectra of all compounds were recorded in either chloroform or dichloromethane as solvent and their λ_{max} values along with the extinction coefficients are presented in Table 5. The UV spectrum of **I** displays three absorption bands at 285 nm, 268 nm and 228 nm. These can be assigned to $n \rightarrow \pi^*$, $\pi \rightarrow \pi^*$ and $\varphi \rightarrow \varphi^*$ transitions. These bands are also present in all complexes, but at slightly shifted λ_{max} values. In addition, all the complexes also display a medium intensity shoulder band around 300–350 nm resulting from charge transfer (CT) transitions. The low energy broad bands appearing around 500–670 nm in all complexes are assigned to CT bands of phenolate to vanadium ($d\pi$), being also characteristic of $V^V O$–aminobisphenol complexes.[8]

Table 5 UV–Vis spectral data for the V^V–compounds obtained in this work.

S.No.	Compound	Solvent	λ_{max}/nm (ε M^{-1}cm^{-1})
1.	$[V^V O(acac)(L^1)]$ **1**	CHCl$_3$	667 (3423), 508 (1973), 384 (1222), 333 (4345), 283 (15580), 262 (18159)
2.	$[V^V O(OMe)(MeOH)(L^1)]$ **2**	CHCl$_3$	670 (1466), 328 (2643), 280 (9825), 266 (10875)
3.	$[\{V^V O(L^1)\}_2\mu–O]$ **3**	CHCl$_3$	576 (2451), 364 (11394), 308 (20034), 279 (26428), 267 (28956),241 (31785)
4.	$H[V^V O_2(L^2)]$ **4**	DCM	609 (1240), 522 (1237), 344 (22011), 269 (17085), 229 (29568)
5.	$[\{V^V O(L^2)\}_2\mu–(OH)_2]$ **5**	DCM	628 (4074), 518 (3622), 310 (14605), 278 (16628), 227 (24952)
6.	$[\{V^V O(L^2)\}_2\mu–O]$ **6**	DCM	620 (2382), 518 (2214), 347 (18175), 273 (23138), 230 (32081)

^{1}H NMR Studies

The modes of coordination in the V^V–complexes were also confirmed by ^{1}H NMR spectral studies. ^{1}H NMR spectra were recorded in CDCl$_3$ and the data are presented in Table S1. A broad signal appearing at δ 9.6 ppm for the two phenolic –OH in the spectrum of **I** is not

detected in the V^V–complexes, indicating deprotonation and coordination of the two phenolic O–atoms. The spectrum of the methoxido compound **2** is complex due to the presence of the two isomeric forms (see ^{51}V NMR description for more details), and thus the number of protons could not be integrated.

The methylenic protons connecting the tripodal N–atom with the phenyl rings becomes diastereotopic upon coordination. Thus, the singlet corresponding to the four methylene protons in the spectrum of the ligand at 3.8 ppm, appears at 2.9 ppm and 3.41– 3.44 ppm in **1**. The spectrum of **1** displays additional signals at 5.6 ppm (1H) and a singlet at 1.9 ppm (6H) corresponding to the coordinated acetylacetonato moiety. Signals for aromatic protons for ligand and complexes resonate well within the expected region, but those of the complexes are significantly up-shielded, probably due to anisotropy of the phenol rings.[8] The proton adjacent to the pyridyl N–atom has an up-field shift of –0.364 ppm {$\Delta\delta = [\delta(complex) - \delta(ligand)]$} in **1**. However, the same proton appears to be remarkably down-shielded in **3** with $\Delta\delta = 1.035$ ppm, probably due to the coordination of pyridyl-N atom to vanadium. Also, the pair of diastereotopic methylene protons in **3,** in special proximity with the coordinated pyridyl–N atom, appears significantly deshielded and resonates as a doublet at an unusually high δ value of 6.00–6.03 ppm, while the other set resonates similarly to that of **1** ($\delta = 3.21$– 3.24 ppm). Complexes **5** and **6** bearing ligand L^2 also exhibit similar resonances, with additional peaks around $\delta = 4.58$ and 4.19 ppm corresponding to the secondary amine protons. The spectrum of **5** exhibits two broad signals at 3.06 ppm and 3.23 ppm assigned to the bridging hydroxide groups.
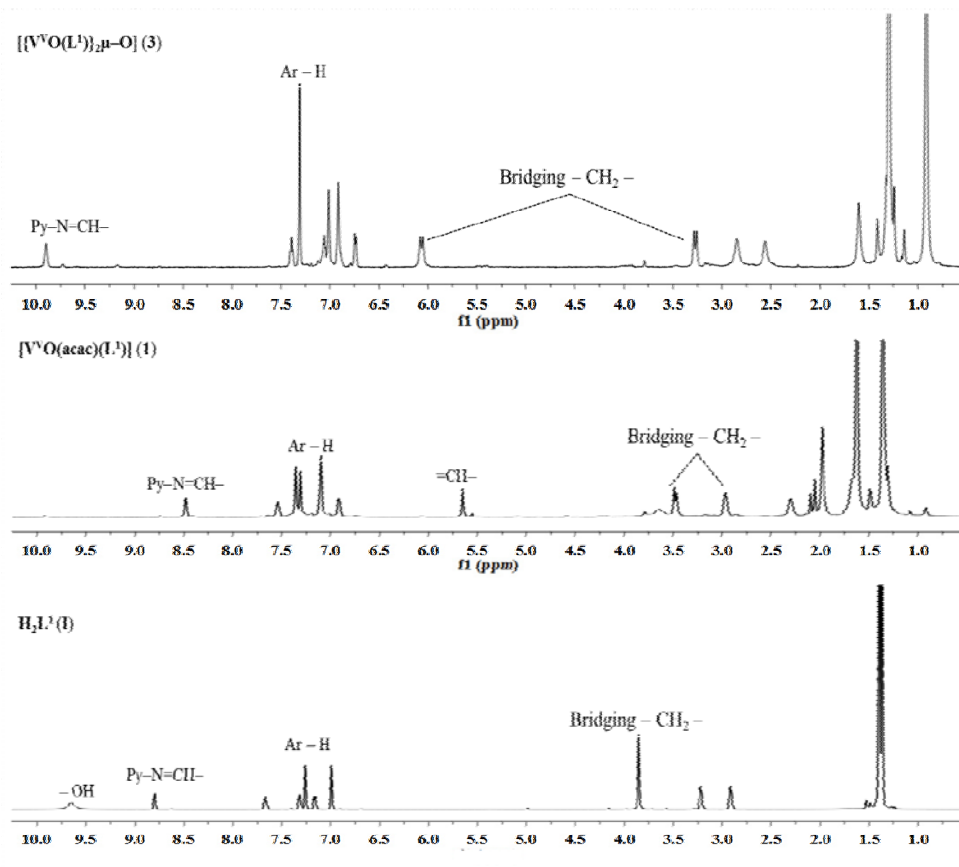
Fig. 6 ^{1}H NMR spectra of H_2L^1 **I**, $[V^VO(acac)(L^1)]$ **1** and $[\{V^VO(L^1)\}_2\mu–O]$ **3** recorded in CDCl$_3$.

^{13}C NMR Studies

The binding modes of the ligands were further supported by the study of the coordination–induced ^{13}C NMR chemical shifts. The spectra were recorded in CDCl$_3$ and the relevant data are presented in Table 6. Significant downfield shifts, $\Delta\delta = [\delta(\text{complex}) – \delta(\text{ligand})]$, were observed in the signals of the carbon atoms in the vicinity of the coordinating atoms. Thus the phenolic carbons become diastereotopic following coordination and appear as two distinct signals with $\Delta\delta$ values varying between 15.93 to 10.09 ppm. The carbons of the pyridine ring in **1** appear similar to those of the ligand, however, the coordination of pyridine N–atom in **3** leads to stark differences in geometry, and this is reflected in the greater $\Delta\delta$ values observed for **3**. The carbons adjacent to the pyridine-N atom suffer significant downfield shifts ($\Delta\delta =$ 14.29 ppm for C5 and 7.68 ppm for C1), due to its coordination. The signals due to the pyridyl ring are not present in compounds **5** and **6** because of the elimination of the

ethylpyridine fragment. Also the carbons C18/C19 become enantiotopic owing to symmetry and thus appear as a singlet around 51.30–59.30 ppm.

Table 6 ^{13}C NMR data for some of the compounds prepared.
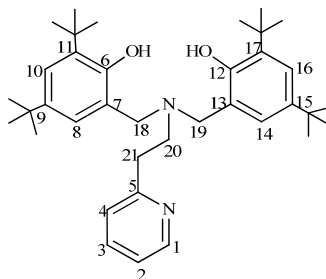
Compound	C1	C5	C6/C12		C9/C15/C11/C17	C18/C19	C20/C21	*tert*–butyl
I	153.11	159.08	148.97		136.21	57.01, 54.09	35.04, 34.81	31.81, 9.74
1 (Δδ) [a]	153.08 (-0.03)	160.49 (1.41)	159.06 149.35	(10.09),	137.54, 136.39, 136.18, 135.96	56.98 (–0.03), 54.05 (–0.04)	35.52, 35.01	30.37, 9.70
3 (Δδ)	160.79 (7.68)	173.37 (14.29)	153.60 148.95	(4.63),	136.72, 134.40	65.72 (8.71), 55.09 (1.00)	34.64, 34.32	29.67, 1.76
5 (Δδ)	–	–	164.88 145.6	(15.91),	135.60, 128.75	59.30 (2.29)	–	29.93, 1.67, 34.68, 5.40
6 (Δδ)	–	–	164.83 145.55	(15.93),	135.55, 134.33	51.30 (-5.71)	–	29.86, 31.58, 31.62, 35.32

[a] Δδ = [δ(complex) – δ(ligand)]

[51]V NMR Studies

The [51]V NMR resonances of the V[V]–compounds were measured in CD_2Cl_2 solution and the spectra obtained are included in the Supporting Information section (Figs. S4–S8). The [51]V NMR spectrum obtained for compound **2** is presented in Figure 7 as an example. The respective experimental chemical shifts are listed in Table 7.

Table 7 Experimental [51]V NMR chemical shifts for **1**, **2**, **3** and **6** in CD_2Cl_2 solution.

Compound	δ_V (ppm)
1	– 455.4 (major), –470
2	– 445 , –455 , –470 (major), – 500, –517.1 (2nd major)
3	–454, –470.1 (major), –514
6	–421.6 (3rd major), –514, –548, -560.5 (2nd major), –579.1 (major)
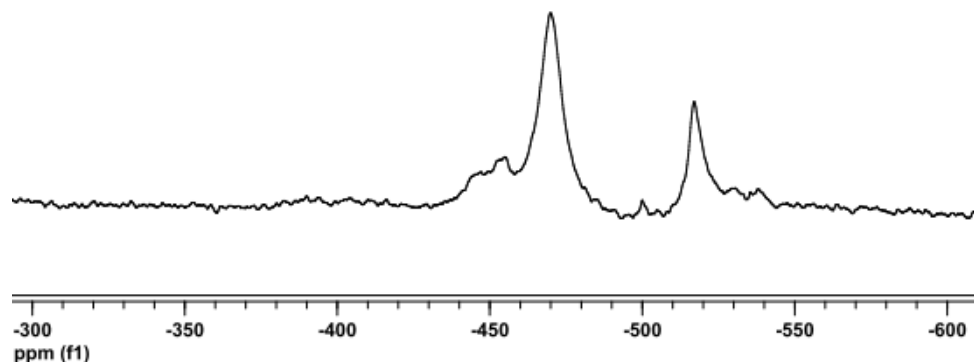
Fig. 7. ^{51}V NMR spectrum of **2** in CD_2Cl_2. There are two major resonances at δ_V = -470 and -517 ppm and several other minor resonances, some of them specified in Table 7.

Compound **1** exhibits two resonances at –455 and –470 ppm which are comparable to those reported for similar V^VO complexes.[8,36] These signals may be due to the likely V^VO conformers present in CD_2Cl_2 solution bearing the following donor atom sets: i) $V^VO[O_{ArO},N_{amine},O_{ArO},O_{acac}]_{eq}[O_{acac}]_{axial}$ ii) $V^VO[O_{ArO},O_{ArO},O_{acac},O_{acac}]_{eq}[N_{amine}]_{axial}$ and iii) $V^VO[O_{ArO},N_{amine},O_{acac},O_{acac}]_{eq}[O_{ArO}]_{axial}$. For the resonance at – 470 ppm, it is plausible that it might correspond to *e.g.* $V^VO[O_{ArO},O_{ArO},O_{MeOH},O_{MeOH}][N_{amine}]_{axial}$. In fact some small amount of solvent might be present, and a similar band is the major one in the ^{51}V NMR spectra of **2** and **3**.

In the case of **2**, where the acac$^-$ ligand is replaced by the monodentate methoxido and methanol ligands, the possibility of additional conformational arrangements is favored. Therefore, in addition to the signals at –454 and –470 ppm, two other signals at –445 and –517 ppm are present. These four signals may be due to the following V^VO species present in solution: i) $V^VO[O_{ArO},N_{amine},O_{ArO},O_{MeO}]_{eq}[O_{MeOH}]_{axial}$; ii) $V^VO[O_{ArO},N_{amine},O_{ArO},O_{MeOH}]_{eq}[O_{MeO}]_{axial}$; iii) $V^VO[O_{ArO},N_{amine},O_{MeOH},O_{MeO}]_{eq}[O_{ArO}]_{axial}$ and iv) $V^VO[O_{ArO},O_{MeOH},O_{ArO},O_{MeO}]_{eq}[N_{amine}]_{axial}$. In addition, species such as $V^VO[O_{ArO},N_{py},O_{ArO},O_{MeO}]_{eq}[N_{amine}]_{axial}$ and $V^VO[O_{ArO},N_{amine},O_{ArO},O_{MeO}]_{eq}[N_{py}]_{axial}$, where the N-pyridine donor atom displaces the methanol ligand may also be considered.

25

The spectrum of the μ–oxido compound **3** resembles that obtained for **2**. In this case, possible binding sets for species present in solution are: i) $V^VO[O_{ArO},N_{amine},O_{ArO},O_{\mu–O}]_{eq}[N_{py}]_{axial}$; ii) $V^VO[O_{ArO},N_{py},O_{ArO},O_{\mu–O}]_{eq}[N_{amine}]_{axial}$ and iii) $V^VO[N_{py},N_{amine},O_{ArO},O_{\mu–O}]_{eq}[O_{ArO}]_{axial}$.

The spectrum obtained for **6** differs significantly from those of **1**, **2** and **3**. In fact, complex **6** involves a distinct ligand, which acts as tridentate, allowing the binding of additional monodentate ligands such as μ–oxido and water. Indeed, two major signals are shifted up-field (–560 and –579 ppm) compared to the single major species obtained for L^1, a tetradentate ligand. This is possibly due to the more electronegative character of O–donor atoms relative to the N–donors of pyridines [37], but this may be a rather simplified view, as the complexes differ significantly, and other factors may also be relevant. In the case of **6** plausible binding sets are: $V^VO[O_{ArO},N_{amine},O_{ArO},O_{\mu–O}]_{eq}[O_{water}]_{axial}$; ii) $V^VO[O_{ArO},N_{py},O_{ArO},O_{water}]_{eq}[O_{\mu–O}]_{axial}$ and a $V=O\cdots V=O$ dimer such as iii) $V^VO[N_{amine},O_{ArO},O_{V=O},O_{\mu–O}]_{eq}[O_{ArO}]_{axial}$.

Reactivity with H_2O_2

Reactivity of complex **1** towards H_2O_2 was monitored by UV–vis spectroscopy upon progressive additions of a H_2O_2 solution (2.22×10^{-2} M, 10.0 mL MeOH) to 25.0 mL of a ca. 1.66×10^{-4} M solution of $[V^VO(acac)(L^1)]$ **1** in $CHCl_3$. Two sets of spectral changes were observed. As shown in Fig. 8, after addition of ca. 500 µL of the above H_2O_2 solution, the bands at 674 and 525 nm gradually decrease in intensity and finally become weak shoulders, while the band at 326 nm decreases in intensity; the changes observed result in the presence of two isosbestic points at 457 nm and 345 nm (Fig. 8a). These spectral changes may be attributed to formation of the corresponding $V^VO–(O_2)$ species through $[V^VO_2]^+$ species. Further additions of H_2O_2, ca. 500 µL, result in the shifts of 326 nm band to 335 nm and the generation of a band at 405 nm along with the formation of an isosbestic point at 476 nm (Fig. 8b). The ^{51}V NMR spectrum recorded in a 3:2 CH_3OH/CD_3OD mixture indicated that weak peaks at –521, –543 and –546 ppm formed upon dissolution of **1** (0.61 mM) in methanol, and the solution acquired a brown coloration. Upon addition of 1 equivalent of H_2O_2 the coloration changed from brown to light yellow and the respective ^{51}V NMR spectrum showed a new species with δ_V at –645 ppm (Fig S7). This chemical shift is characteristic of inorganic $[V^VO–(O_2)]$–type species[38], thus it is probably due either to $HVO_3(O_2)^{2–}$ or to a peroxido complex derived from **1**.

(a)   (b)
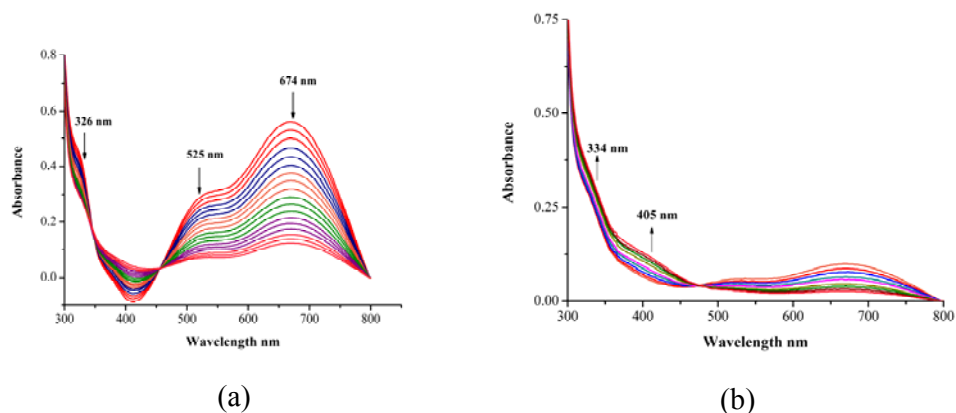
Fig. 8 Two sequential sets (a) and (b) of spectral changes obtained by progressive additions of a H_2O_2 solution $((2.22 \times 10^{-2}$ M) of 30% H_2O_2 dissolved in 10.0 mL of MeOH) to 25.0 mL of a ca. 1.66×10^{-4} M solution of $[V^VO(acac)(L^1)]$ **1** in $CHCl_3$.

We also monitored the spectral changes (in the visible range if any) during the conversion of $[V^VO(acac)(L^1)]$ **1** into the dinuclear $[\{V^VO(L^1)\}_2\mu–O]$ **3** in acetonitrile (see experimental section) over a period of 7 days. The resulting spectral changes do not confer much information, since no new distinct band was generated in the spectra during this period. Notwithstanding, the intensity of bands at 674 and 525 nm initially increased (during the first 7 h), and then decreased only slightly with time; Fig 9. The existence of an isosbestic point at ca. 490 nm suggests the existence of the two complexes (**1** and **3**) in equilibrium in solution. Upon standing the solution at ca. 0 ˚C, the major product **1** crystallizes out from the solution, while at room temperature the equilibrium slowly moves towards **3**.
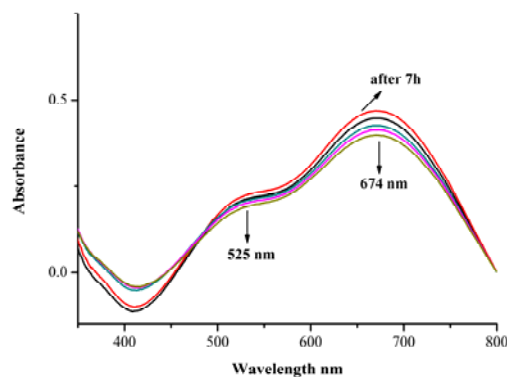
Fig. 9 Spectral changes observed in the electronic spectrum of $[V^VO(acac)(L^1)]$ **1** in MeCN with time.

27

The addition of a H_2O_2 solution (2.22×10^{-2} M, 10.0 mL MeCN) to a solution of **1** (25.0 mL of a ca. 1.16×10^{-4} M solution in acetonitrile) also showed a similar trend, i.e. an initial increase in the intensity of the 674, 525 nm and 326 nm bands. This trend continued till the addition of ca. 2.1 mL of the H_2O_2 solution; Fig. 10a. These changes also resulted in the observation of two isosbestic points at 434 nm and at 389 nm. Further additions of H_2O_2 yielded only a small decrease in intensity for all three bands in the spectra. After addition of ca. 500 μL of H_2O_2 solution, the system stabilized, and showed no further H_2O_2 effect [Fig. 10b]. Thus, the two bands at 674 and 525 nm, which almost disappeared in MeOH/CHCl$_3$ solution, are still present when a similar experiment was done in acetonitrile. In contrast to what was observed in methanol, there was no observable change either in sample coloration (dark blue) or in the respective ^{51}V NMR spectrum of **1** in 3:2 CH$_3$CN/CD$_3$CN mixture (0.62 mM), even after the addition of 8 equivalents of H_2O_2 (see Fig. S8). This also indicates that **1** is much more resistant to dissociation in the presence of H_2O_2 when in polar aprotic medium.

Spectral changes observed by sequential addition of a solution of H_2O_2 in MeCN to a solution of $[V^VO(OMe)(MeOH)(L^1)]$ **2** in MeCN are shown in Fig. 11. The intensity of the 670 nm band decreases gradually and finally becomes flat. Simultaneously a new clearly distinct band generates at 460 nm. Since no other bidentate ligand (like in **1**) is present in this complex, we may conclude that **2** forms the peroxido complex in solution. In fact, the $V^VO(O_2)$ complex was reported to have a band with λ_{max} = 455 nm in aqueous acidic medium.[39,40] Unlike what was observed for the ^{51}V NMR spectrum of **1** in 3:2 CH$_3$CN/CD$_3$CN, there was a significant change either in sample coloration (dark blue) and in the respective ^{51}V NMR spectrum of **2** in 3:2 CH$_3$CN/CD$_3$CN mixture (2.3 mM) after the addition of 8 equivalents of H_2O_2 (see Fig. 12). A weak signal appears at –542 ppm after the addition of 1 equivalent of H_2O_2, but the $V^VO(O_2)$–L^2–type species formed (resonances at –585, –595 and 603 ppm) and the ligand free inorganic $V^VO(O_2)_2$–type species (resonances at –698 and –707 ppm) are only detected after the addition of 8 equivalents of H_2O_2.[38,41] The presence of signals beyond –600 ppm, typical of $V^VO(O_2)$–type species, indicates that **2**, when in polar aprotic medium, is not as resistant to dissociation as compound **1** in the presence of H_2O_2. All ^{51}V NMR signals disappear ~72 h after the addition of oxidant.

(a)   (b)
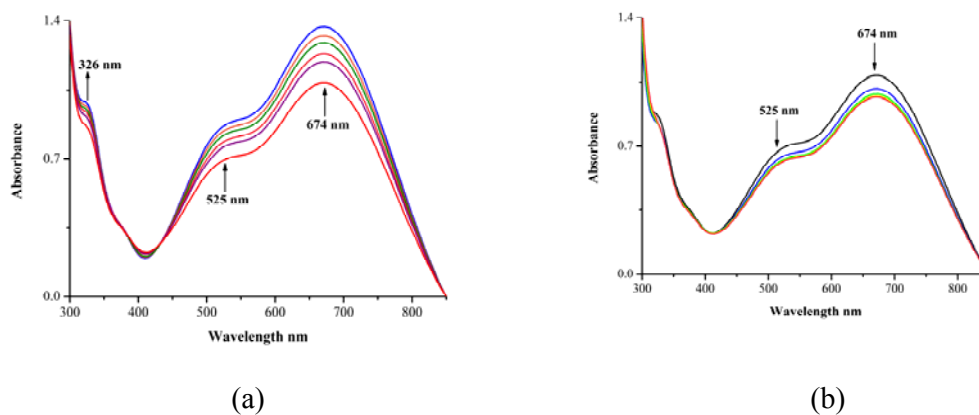
Fig. 10 Two sequential sets (a) and (b) of spectral changes obtained by progressive additions of a H_2O_2 solution (2.22×10^{-2} M, of 30 % H_2O_2 dissolved in 10.0 mL of MeCN) to 25.0 mL of a ca. 1.16×10^{-4} M solution of $[V^VO(acac)(L^1)]$ **1** in MeCN.
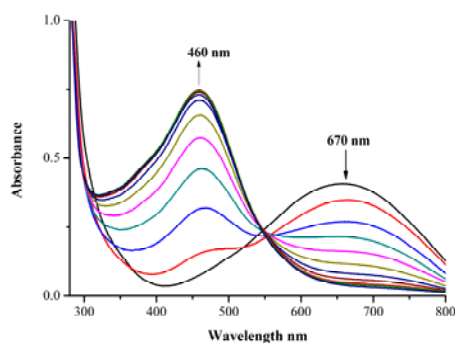
Fig. 11 Spectral changes obtained by progressive additions of a H_2O_2 solution (2.22×10^{-2} M) to 15.0 mL of a ca. 1.23×10^{-4} M solution of $[V^VO(OMe)(MeOH)(L^1)]$ **2** in MeCN.
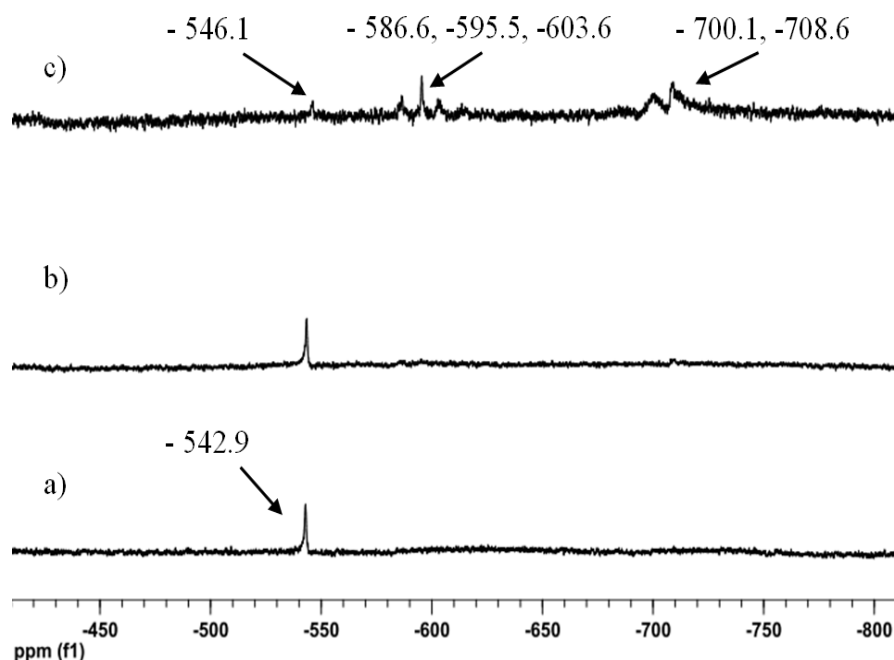
Fig. 12 ^{51}V NMR spectra of **2** in 3:2 CH_3CN/CD_3CN mixture and in the presence of : a) 1 equivalent of H_2O_2; b) 2 equivalents of H_2O_2 and c) 8 equivalents of H_2O_2.

Catechol Oxidase Mimetic Activity: catalytic oxidation of catechol

The catechol oxidase mimetic activity of the system containing $[V^VO(OMe)(MeOH)(L^1)]$ **2** was studied by using catechol as the substrate in an air atmosphere. Catechol oxidase like oxidation of catechol yields o–benzoquinone (Scheme 2), with a characteristic absorbance at 383 nm. Thus, the reaction can be followed by monitoring the absorbance increase at 383 nm.
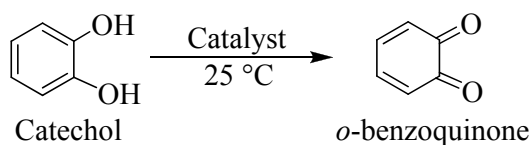
Scheme 2 Oxidation of catechol to o–benzoquinone.

The reaction was initiated with the addition of 5.0 mL of a 3.9834×10^{-4} M solution of $[V^VO(OMe)(MeOH)(L^1)]$ to a 10.0 mL (1.0000×10^{-1} M) solution of catechol, maintained at 25 °C. The reaction was followed by recording the UV–Vis spectra after every 3 minutes. After about 10 sec of preparation the mixture of the complex and catechol turned dark blue, indicating the coordination of catecholate to vanadium. This is also evident from the strong

absorptions appearing at 614 nm and 916 nm, which is characteristic of charge transfer bands in vanadium catecholate–containing complexes.[25,26,42]

Catecholates form non-innocent complexes with vanadium(V), often a reduction ($V^V \rightarrow V^{IV}$) occurring.[43] Namely some of us reported a group of non-innocent mixed-ligand oxidovanadium(V) complexes some of them including the catecholate ligand[44]. Many V^V–catechol complexes have been prepared and often they are unstable with respect to internal redox reactions.[42,45,46] It is also known that *o*–benzoquinones may form from these systems[47] and V^{III}–, V^{IV}– and V^V–catechol complexes have been characterized. Stable V–catechol compounds can be prepared without change in V–oxidation state in aprotic media, but in protic media, e.g. MeOH or H_2O, the systems often yield V^V–species.[48]

The catechol oxidase activity was evaluated both in an atmosphere of air as well as under molecular dioxygen (Figs. 15, 16 and 17). The activity is comparable in both cases, being slightly higher in the presence of molecular oxygen (Fig. 17). As the reaction progresses, the bands at 614 nm and 916 nm firstly decrease in intensity and finally approximately stabilize (Fig. 16), while the band at 383 nm continues to increase with time (Fig. 15). During the process, the formed vanadium complex containing catecholate releases the oxidised product, *o*–benzoquinone, and reacts with another molecule of catechol to yield back the vanadium complex containing catecholate, thereby continuing the catalytic cycle. Re–oxidation of the generated V^{III} or V^{IV} species by O_2 must take place in order to restart the catalytic cycle. This step may occur prior to the coordination of the substrate or it may be a concerted process (see also below). Overall, this may be a two–electron V^V/V^{III} process, with water being the likely by–product.[49] Consequently the concentration of the vanadium complex containing catecholate probably remains constant during the reaction, which is also reflected by the approximately constant absorbance at 614 nm and 916 nm observed after ~60 min. On the other hand the absorbance at 383 nm increases progressively, with increase in quinone amount during the course of reaction. The coordination of catecholate was further substantiated by recording the ESI–MS spectrum for the above mentioned reaction mixture. The low intensity peak at 771.92 may be attributed to the formation of $[V^VO(cat)(HL^1)K]^+$ species (calc. 771.33) (Fig. S9).

We observed striking differences between the reactivity of catechol and 3,5–di–*tert*–butyl catechol with **2**. The 3,5–di–*tert*–butyl catechol (DTBC) is a substrate of choice of many researchers for evaluating catechol oxidase activity.[11,12] However, we observed a very slow reaction when using DTBC as substrate in dilute concentrations, and practically no

reaction in concentrated solutions (Fig. S10). The generation of two new bands around 646 nm and 898 nm in the solution containing DTBC mixed with 1000 times dilute $[V^VO(OMe)(MeOH)(L^1)]$ indicates coordination of DTBC to vanadium similarly to catechol,[42,48] but the intensity of these bands continue to increase with time.

Redox chemistry of V–catechol compounds is complex, also depending on the substituents of the catechol,[42,45,46] and in protic media containing DTBC it was concluded that metal oxidation occurs before ligand oxidation, V^V–DTBC complexes being formed.[48] The reasons for the presently observed distinct behaviour of catechol and DTBC are not clear, but we may hypothesise that steric bulkiness of this substrate may hinder the approach/coordination of the substrate to the V–site, this accounting for the lower reactivity. Conversely, once the electron transfer occurred and the quinone is formed, dissociation from the V–centre should be facilitated. In addition, electron donating substituents on the substrate structure will lower the quinone/catechol redox potential, thus making it harder to carry out this reaction with DTBC under the same conditions used for catechol. This might explain why the V–catecholate complex continues to form and the quinone amounts remain minimal. The V^V/V^{IV} and V^{III}/V^{IV} redox potentials of these complexes should be taken into account to fully understand the distinct behaviour observed.[50,51] Notwithstanding, the concentration of V–DTBC complex continues to slowly increase with time which is evident from the progressive rise in 646 and 898 nm bands, while only a weak quinone band is generated at 373 nm (Fig. S10). These λ_{max} values differ significantly from those of V–DTBC complexes,[48] thus most probably in this system the complex formed also contains ligand L^1 in its coordination sphere.

Additional studies were carried out by X–Band EPR and NMR with the purpose of detecting any paramagnetic V species generated in reaction mixtures of **2** and catechol. Indeed, a V^{IV}–species is formed by the reaction of **2** (13 mM in a 3:2 mixture of CH_3OH/CD_3OD with 0.91 M of t-butyl alcohol) with an excess of catechol (Fig. 13).

Non–oxido V^{IV} complexes have been studied, namely by the group of Garribba.[52] In the more recent study[52(a)] the authors give an explanation for the relatively low values of hyperfine coupling constant A_i (A_i corresponds to the higher of the A_z, A_x or A_y measured for the non–oxido V^{IV} species). This is related to the mixing of V–d_{xy} with the excited V–d_{xz}, V–d_{yz} and V–d_{z2} orbitals.

Literature reports indicate that the removal of the oxido ligand from the $V^{IV}O$ moiety can occur in the presence of catecholate–type ligands[42,48,53] and in the present case the g and A parameters obtained (g_i =1.958 and A_i = 137×10^{-4} cm^{-1}) significantly differ from those reported for V^{IV}–catecholato systems[54] $V^{IV}O(cat)$ (g_z =1.943, A_z = 170×10^{-4} cm^{-1}), $V^{IV}O(cat)_2{}^{2-}$ (g_z =1.947, A_z = 154×10^{-4} cm^{-1}) and $V^{IV}(cat)_3{}^{2-}$ ($g_{x,y}$ = 1.937, $A_{x,y}$ = 107×10^{-4} cm^{-1}, g_z = 1.991, A_z = 14×10^{-4} cm^{-1}). The spin Hamiltonian parameters obtained by simulation of the experimental EPR spectrum in the present system are thus consistent with the formation of a non-oxido V^{IV} species such as $V^{IV}[(L^1)(cat)]$ (noteworthy is also the fact that a $[V^{V}O(cat)(HL^1)K]^+$ species was detected by ESI–MS, see above). Additionally, the value of A experimentally measured for this non–oxido species is significantly higher than the V^{IV} species formed by dithiocarbazate ONS ligands (ca. 120.0×10^{-4} cm^{-1})[52(a)], as well as for V(Cat)$_3$ ($A_{x,y}$ = 107×10^{-4} cm^{-1})[54] are in agreement with a higher V–d_{xy} contribution to the SOMO (singly occupied molecular orbital) in the present case.

Vanadium species in the V^{III} oxidation state may also form, but typically V^{III}–complexes are not detected by X–band EPR. The measurement of magnetic susceptibility by NMR could provide some indication regarding the presence of V^{III} in solution. However, unexpectedly a negative (diamagnetic) sample shift, relative the internal reference sample (0.91 M of t–butyl alcohol in a 3:2 of CH$_3$OH/CD$_3$OD), was obtained. This diamagnetic shift may be due to the high concentration of catechol present in the sample.
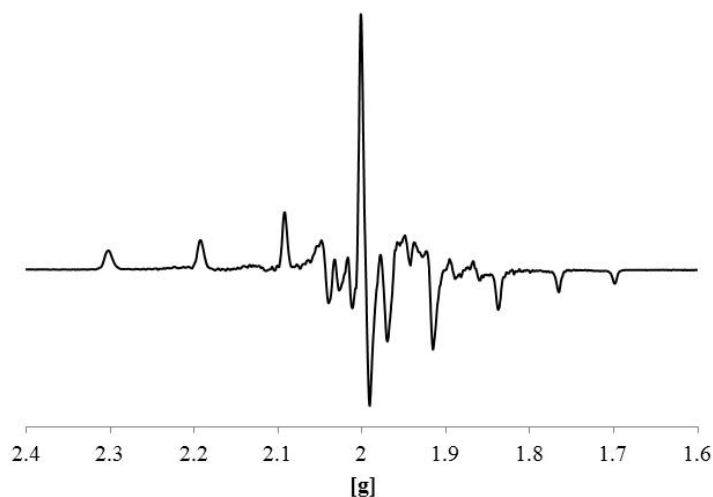
Fig. 13. First derivative of the X–band EPR spectrum of the V^{IV} species formed by the reaction of **2** (13.1 mM) with catechol (480 mM) in a 3:2 mixture of CH$_3$OH/CD$_3$OD with

0.91 M of *tert*–butyl alcohol, at room temperature and after 72 h. This spectrum was simulated by using the program of Rockenbauer and Korecz.[20]

To evaluate the catechol oxidase mimetic activity of $[V^VO(OMe)(MeOH)(L^1)]$, steady state kinetic studies were carried out in MeOH and kinetic parameters, V_{max}, K_M, and k_{cat} were determined assuming a Michaelis–Menten behaviour for the system. The Michaelis–Menten equation for a single substrate reaction may be expressed as

$$V_i = V_{max} \times \frac{[S]}{K_M + [S]}$$

Where V_i is the initial reaction velocity and [S] is the substrate concentration.

Different concentrations of catechol solution (0.0250 – 0.1750 M), were added to a 3.9834×10^{-4} M solution of $[V^VO(OMe)(MeOH)(L^1)]$ in an air atmosphere. For each substrate–complex mixture the spectra were recorded after 3 min of preparation for a period of 3 min. Initial rates were obtained from linear regression of absorbance versus time plots; Fig. 14. The experiments were run in duplicates and their average was used for the calculations. The initial rates and the substrate concentrations were then fitted to the Michaelis–Menten equation via non–linear regression analysis using Origin 8.0 software. The oxidation of DTBC was too slow to allow similar kinetic studies.

It was observed that the system containing $[V^VO(OMe)(MeOH)(L^1)]$ follows a Michaelis–Menten like kinetics. The rate of reaction follows the first order kinetics at low substrate concentration, with a linear velocity versus time graph; Fig. 14. As frequently found in similar studies with enzymes, as the substrate concentration increases, the catalyst gets saturated and consequently the reaction rate becomes independent of substrate concentration; hence the reaction becomes zero order with respect to substrate concentration. Thus, we may consider that the present system follows a Michaelis–Menten type kinetics with respect to catechol. The obtained V_{max} and K_M values are 7.66×10^{-6} M min^{-1} and 0.0557 M, respectively. k_{cat} (turn over frequency) was calculated by using the following formula:

$$k_{cat} \text{ (TOF) } = \frac{\text{amount of substrate consumed}}{\text{unit time} \times \text{unit mole of catalyst}}$$

k_{cat} being 0.0541 min^{-1}.
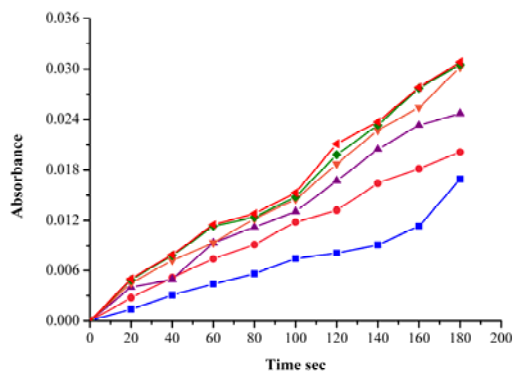
Fig. 14 Change of absorbance at 383 nm versus time for the solutions used for kinetic studies monitored after 3 min of preparation.
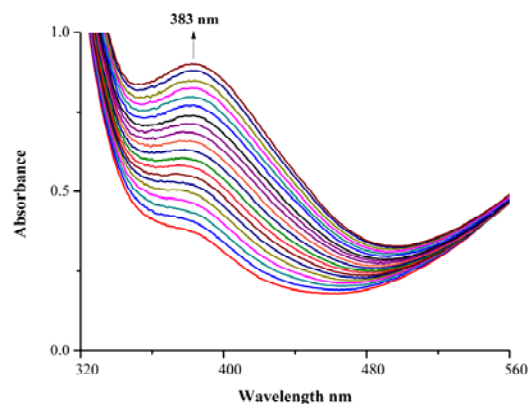
Fig. 15 Increase in absorbance at 383 nm with time. The spectra are recorded at every 3 min intervals. Reaction conditions: catechol solution (10.0 mL, 1.00×10^{-1} M) mixed with 5.0 mL of a 3.9834×10^{-4} M solution of $[V^{V}O(OMe)(MeOH)(L^{1})]$ **2** in an atmosphere of air.
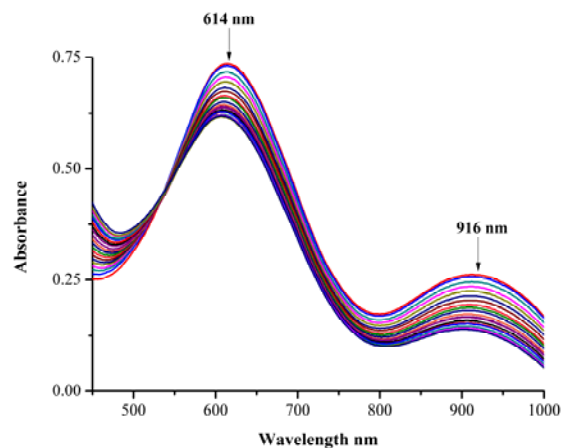
Fig. 16 Spectral changes observed for the absorbance at 614 nm and 916 nm with time. The spectra were recorded at every 3 min intervals. Reaction conditions: catechol solution (10.0 mL, 1.00×10^{-1} M) mixed with 5.0 mL of a 3.9834×10^{-4} M solution of [$V^VO(OMe)(MeOH)(L^1)$] **2** in an atmosphere of air.
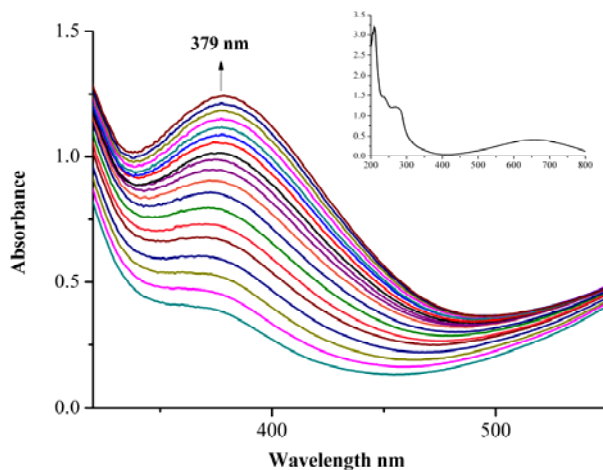
Fig. 17 Increase in absorbance at 379 nm with time. The spectra were recorded at every 3 min intervals. Reaction conditions: catechol solution (10.0 mL, 1.00×10^{-1} M) mixed with 5.0 mL of a 3.9834×10^{-4} M solution of [$V^VO(OMe)(MeOH)(L^1)$] **2** in an atmosphere of molecular oxygen. Inset: UV–Visible spectrum of [$V^VO(OMe)(MeOH)(L^1)$] **2** in MeOH**.**
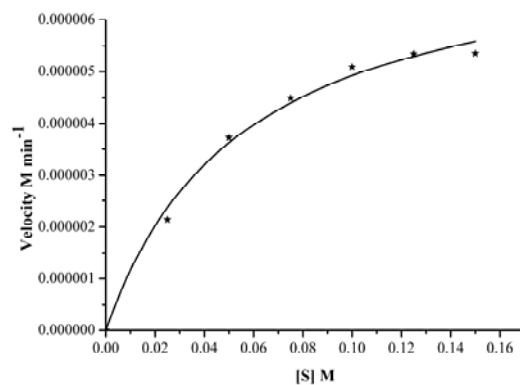
Fig. 18 Plot of velocity versus substrate concentration for complex **2** (see text for details).

Table 8 V_{max}, K_M and k_{cat} values for complex **2.**

V_{max} (M min^{-1})	K_M (mM)	k_{cat}
7.66×10^{-6}	55.7	3.24 h^{-1}
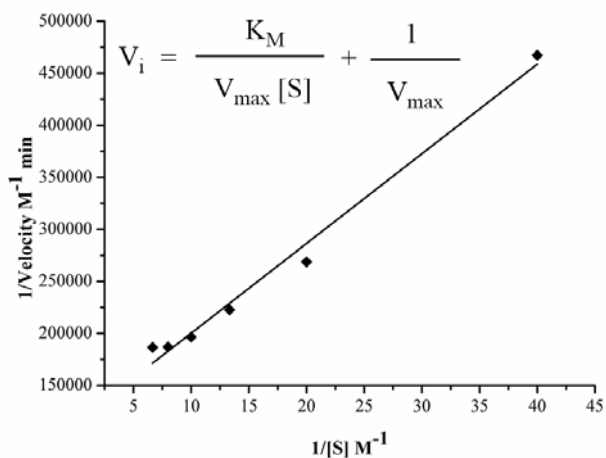
Fig. 19 Lineweaver–Burk Plot for complex **2**.

Oxidative bromination of thymol

Mononuclear V^V–amine trisphenolate complexes have been reported to be good structural and functional models of VHPOs, catalyzing the oxidation, with H_2O_2 of thioethers and Br$^-$

ions.[55] The oxidative bromination of thymol has been much less studied. [56, 57] Here this reaction was carried out in aqueous medium and gave three different products, namely, 2–bromothymol, 4–bromothymol and 2,4–dibromothymol. The products formed were the same as in previous studies by some of us[56] and by other authors[57]; Scheme 3.

o-MBrP   p-MBrP   DBrP
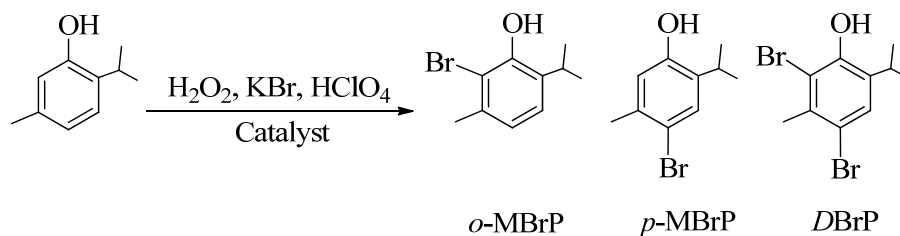
Scheme 3 Products obtained in the oxidative bromination of thymol carried out in aqueous medium using **2** as catalyst precursor.

For the chosen complex, $[V^VO(OMe)(MeOH)(L^1)]$ **2** (0.0010 g), used as the catalyst precursor, the following parameters were varied to optimize the reaction conditions for 10.0 mmol (1.500 g) of thymol, namely (i) amount of $HClO_4$ (10.0 and 20.0 mmol) (ii) amount of KBr (10.0 and 20.0 mmol), and (iii) amount of oxidant, H_2O_2 (10.0 and 20.0 mmol). Table 9 presents the details of conversion under each specified condition. The best suited conditions for the maximum conversion of 10.0 mmol of thymol (1.500 g) were: KBr (2.380 g, 20.0 mmol), aqueous 30% H_2O_2 (2.267 g, 20.0 mmol), $HClO_4$ (20.0 mmol, added in four equal portions of 0.717 g) and 20.0 mL water. After 2 h of reaction time, a maximum of 99 % conversion was achieved.

This reaction mimics those catalysed by some vanadium haloperoxidases.[30,57,58] In the particular case of this system containing compound **2**, confirmed here to behave as a functional model of VHPOs, it is probable that the intermediate involved in the catalytic cycle is a peroxide complex of type $V^VO(O_2)(H_nL^2)$. The formation of such species was confirmed (e.g. Fig. 12) by the observation of resonances at –585, –595 and –603 ppm in the ^{51}V NMR spectra of **2** in acetonitrile, upon addition of a H_2O_2 solution.

We cannot exclude that ligand–free peroxido–vanadates may be also taking some participation in the process. However, e.g. Conte and co-workers, in a recent study[57], stated that the inorganic monoperoxido V–complex was more reactive than the diperoxido V–complex toward the oxybromination of alkenes and alkynes. In another report[59], the same group reported that by spectroscopic techniques they were able to identify monoperoxido V–

complexes as the oxidant of the Br⁻ ion, while the diperoxido derivative would act as a reservoir for the active oxidant. Several other reports by the same group[60, 41(a)] globally also appear to lead to the idea that the monoperoxido-type complexes VO–(O₂)–(L) are more active than the inorganic peroxido V compounds. Although most of the publications do not refer to thymol as substrate, we would favor the idea that the VO(O₂)(L)–type species, detected by [51]V NMR, are the active catalysts.

The selectivity of different products showed interesting trends with respect to the amount of H_2O_2 added to the reaction mixture. All the reactions involving one equivalent of H_2O_2 resulted in the formation of only two isomers of mono–brominated products with high selectivity (up to 93 %) for the *para* isomer product (*p*–MBrP) irrespective of the amounts of $HClO_4$ and KBr used in the reaction. However, increasing the H_2O_2 amount to two equivalents, the outcome of the reaction changed significantly giving three products with a preference (57 %) towards the dibromo product DBrP, followed by 37 % towards the *para* mono–brominated isomer.

The selectivity trend found here differs from that recently reported by Conte and co-workers[57] using NH_4VO_3 as catalysts precursor for the oxidation of thymol. Besides the present system appearing as significantly more active than NH_4VO_3, showing significantly higher TOF values, the para–Br–derivative is also the preferred product; at least when using equivalent amounts of H_2O_2 and thymol, in the present case *p*–MBrP forms in quite higher relative amounts.

Table 9 Results of oxidative bromination of thymol (1.50 g, 10.0 mmol) using $[V^VO(OMe)(MeOH)(L^1)]$ **2** as the catalyst precursor after 2 h of reaction time.

Entry No.	KBr	H₂O₂	HClO₄	Catalyst	H₂O	% Conv.	TOF (h⁻¹)	% Selectivity		
	(g, mmol)	(g, mmol)	(g, mmol)	(g)	(mL)			*o*–MBrP	*p*–MBrP	di–BrP
1.	1.19, 10	1.13, 10	1.43, 10	0.0010	20	28	1000	11	89	—
2.	1.19, 10	1.13, 10	2.87, 20	0.0010	20	67	2393	7	93	—
3.	2.38, 20	1.13, 10	2.87, 20	0.0010	20	76	2714	7	93	—
4.	2.38, 20	2.27, 20	2.87, 20	0.0010	20	99	3568	5	37	57

Conclusions

The reaction of the tripodal tetradentate dibasic ligand H_2L^1 with $[V^{IV}O(acac)_2]$ in MeCN gave the V^VO–complex, $[V^VO(acac)(L^1)]$ **1**. This displayed interesting solution behaviour. A solution of **1** after refluxing in MeCN, on cooling to 0 ˚C yielded dark blue crystals of **1**; in contrast a filtered solution of **1** in MeCN at room temperature afforded dark green crystals of $[\{V^VO(L^1)\}_2\mu–O]$ **3**. Prolonged treatment of **1** in MeOH yielded the methoxido compound, $[V^VO(OMe)(MeOH)(L^1)]$ **2**. Refluxing **2** in acetonitrile or acetone also resulted in the dinuclear compound **3**. All the three complexes have a distorted octahedral geometry around vanadium. The phenols coordinate in a *cis* fashion in **1**, but isomerize to *trans* geometry in **2** and **3**.

Reaction of H_2L^1 with $V^{IV}OSO_4$ resulted in partial hydrolysis of the tripodal ligand resulting in the formation of **4** containing the ONO tridentate ligand, H_2L^2, formed by elimination of the ethylpyridine moiety from L^1. Compound **4** undergoes oxidative dimerization in acetone yielding the hydroxide–bridged dimer, $[\{V^VO(L^2)\}_2\mu(HO)_2]$ **5**, having distorted octahedral geometry around each vanadium. However, an acetonitrile solution of **4** yielded black coloured crystals of the dinuclear compound $[\{V^VO(L^2)\}_2\mu–O]$ **6** with trigonal bipyramidal coordination geometry around each vanadium.

The system containing the methoxido complex **2** was successfully employed as a catechol–oxidase functional mimic in the oxidation of catechol to *o*–benzoquinone in air, a reaction that may be considered to follow a Michaelis–Menten type kinetics with respect to catechol. Interestingly the similar reaction with the bulkier 3,5–di–*tert*–butylcatechol proceeded with at much slower rate.

The same catalyst precursor, $[V^VO(OMe)(MeOH)(L^1)]$ **2**, was used for the oxidative bromination of thymol by H_2O_2 in aqueous medium. The products formed were the same as in a previous study using NH_4VO_3 as catalysts precursor[57], but the present system, besides being significantly more active, the selectivity showed quite interesting trends, namely ~93 % for the *para* mono–brominated product, and no dibromo derivative when not using excess of primary oxidizing agent.

References

1. *(a)* J. Costa Pessoa, S. Etcheverry and D. Gambino, *Coord. Chem. Rev.*, 2015, http://dx.doi.org/10.1016/j.ccr.2014.12.002; *(b)* Y. Yoshikawa, H. Sakurai, D. C. Crans, G. Micera and E. Garribba, *Dalton Trans.*, 2014, **43**, 6965–6972; *(c)* T. K. Saha, Y. Yoshikawa, H. Yasui and H. Sakurai, J. *Porphyrins Phthalocyanines*, 2012, **16**, 114–121; *(d)* H. Sakurai, Y.

Yoshikawa and H. Yasui, *Chem. Soc. Rev.*, 2008, **37**, 2383–2392; *(e)* T. Kiss, T. Jakusch, D. Hollender, É. A. Enyedy and L. Horváth, *J. Inorg. Biochem.*, 2009, **103**, 527–535; *(f)* J. Costa Pessoa, E. Garribba, M. F. A. Santos, T. Santos–Silva, Coord. Chem. Rev., 2015, http://dx.doi.org/10.1016/j.ccr.2015.03.016.

2. *(a)* J. Benítez, A. C. de Queiroz, I. Correia, M. A. Alves, M. S. Alexandre–Moreira, E. J. Barreiro, L. M. Lima, J. Varela, M. González, H. Cerecetto, V. Moreno, J. Costa Pessoa and D. Gambino, *Eur. J. Med. Chem.*, 2013, **62**, 20–27; *(b)* L. G. Naso, M. Valcarcel, M. Roura–Ferrer, D. Kortazar, C. Salado, L. Lezama, T. Rojo, A. C. González–Baró, P. A. M. Wiliams and E. G. Ferrer, *J. Inorg. Biochem.*, 2014, **135**, 86–99; *(c)* M. R. Maurya, S. Agarwal, M. Abid, A. Azam, C. Bader, M. Ebel and D. Rehder, *Dalton Trans.*, 2006, 937–947; *(d)* M. R. Maurya, A. A. Khan, A. Azam, S. Ranjan, N. Mondal, A. Kumar, F. Avecilla and J. Costa Pessoa, *Dalton Trans.*, 2010, **39**, 1345–1360; *(e)* M. R. Maurya, A. A. Khan, A. Azam, A. Kumar, S. Ranjan, N. Mondal and J. Costa Pessoa, *Eur. J. Inorg. Chem.*, 2009, 5377–5390; *(f)* M. R. Maurya, C. Haldar, A. A. Khan, A. Azam, A. Salahuddin, A. Kumar and J. Costa Pessoa, *Eur. J. Inorg. Chem.*, 2012, 2560–2577.

3. *(a)* M. R. Maurya, C. Haldar, A. Kumar, M. L. Kuznetsov, F. Avecilla and J. Costa Pessoa, *Dalton Trans.*, 2013, **42**, 11941–11962; *(b)* M. R. Maurya, N. Chaudhary, F. Avecilla, P. Adão and J. Costa Pessoa, *Dalton Trans.*, 2015, **44**, 1121–1232; *(c)* M. R. Maurya, A. Kumar and J. Costa Pessoa, *Coord. Chem. Rev.*, 2011**, 255**, 2315– 2344; *(d)* H. Pellissier, *Coord. Chem. Rev.*, 2015**, 284**, 93–110; *(e)* M. R. Maurya, N. Chaudhary, A. Kumar, F. Avecilla and J. Costa Pessoa, *Inorg. Chim. Acta*, 2014, **420**, 24–38.

4. C. Leblanc, H. Vilter, J. B. Fournier, L. Delage, P. Potin, E. Rebuffet, G. Michel, P. L. Solari, M. C. Feiters and M. Czjzek, *Coord. Chem. Rev.*, http://dx.doi.org/10.1016/j.ccr.2015.02.013.

5. *(a)* J. B. Wang, L. P. Lu, J. Y. Liua and Y. S. Li, *Dalton Trans.*, 2014, **43**, 12926–12934; *(b)* J. Q. Wu, J. S. Mu, S. W. Zhang and Y. S. Li, *J Polymer Science: Part A: Polymer Chem.*, 2010, 48, 1122–1132.

6. *(a)* O. Wichmann, H. Sopo, A. Lehtonen and R. Sillanpää, *Eur. J. Inorg. Chem.*, 2011, 1283–1291; *(b)* D. Maity, A. Ray, W. S. Sheldrick, H. M. Figge, B. Bandyopadhyay and M. Ali, *Inorg. Chim. Acta*, 2006, **359**, 3197–3204; *(d)* T. Kajiwara, R. Wagner, E. Bill, T. Weyhermüller and P. Chaudhuri, *Dalton Trans.*, 2011, **40**, 12719–12726; *(e)* L. H. Tong, Y. L. Wong, H. K. Lee and J. R. Dilworth, *Inorg. Chim. Acta*, 2012**, 383**, 91–97.

7. *(a)* S. Groysman, I. Goldberg, Z. Goldschmidt, M. Kol, *Inorg. Chem*., **2005**, 44, 5073–5080; *(b)* G. Zhang, B. L. Scott, R. Wu, L. A. P. Silks and S. K. Hanson, *Inorg. Chem.*, 2012, **51**, 7354−7361; *(c)* F. Madeira, S. Barroso, S. Namorado, P. M. Reis, B. Royo and A. M. Martins, *Inorg. Chim. Acta*, 2012**, 383**, 152–156; *(d)* N. M. L. Silva, C. B. Pinheiro, E. P. Chacon, J. A. L.C. Resende, J. W. de M. Carneiro, T. L. Fernández, M. Scarpellini, M. Lanznaster, *J. Braz. Chem. Soc.*, 2011, **22**, 660–668.

8. S. Barroso, P. Adão, F. Madeira, M. T. Duarte, J. Costa Pessoa and A. M. Martins, *Inorg. Chem.*, 2010, **49**, 7452–7463.

9. A. A. El-Taras, I. M. EL–Mehasseb, A. E. M. M. Ramadan, *C. R. Chimie.*, 2012, **15**, 298–310.

10. S. K. Dey and A. Mukherjee, *New J. Chem.*, 2014, **38**, 4985–4995.

11. A. Patra, G. C. Giri, T. K. Sen, L. Carrella, S. K. Mandal and M. Bera, *Polyhedron*, 2014, **67**, 495–504.

12. P. Chakraborty, S. Majumder, A. Jana and S. Mohanta, *Inorg. Chim. Acta*, 2014, **410**, 65–75.

13. I. A. Koval, P. Gamez, C. Belle, K. Selmeczi and J. Reedijk, *Chem. Soc. Rev.*, 2006, **35**, 814–840.

14. *(a)* S. Caglar, I. E. Aydemir, E. Adıguzel, B. Caglar, S. Demir and O. Buyukgungor, *Inorg. Chim. Acta*, 2013, **408**, 131–138; *(b)* S. Sarkar, S. Majumder, S. Sasmal, L. Carrella, E. Rentschler and S. Mohanta, *Polyhedron*, 2013, **50**, 270–282; *(c)* S. Anbu, E. C. B. A. Alegria and A. J. L. Pombeiro, *Inorg. Chim. Acta,* 2015, **431**, 139–144; *(d)* M. Shyamal, T. K. Mandal, A. Panja and A. Saha, *RSC Adv.*, 2014, **4**, 53520–53530.

15. *(a)* M. Mitra, A. K. Maji, B. K. Ghosh, P. Raghavaiah, J. Ribas and R. Ghosh, *Polyhedron*, 2014, **67**, 19–26; *(b)* A. Jana, N. A. Alcalde, E. Ruiz and S. Mohanta, *Inorg. Chem.*, 2013, **52**, 7732−7746; *(c)* A. Guha, K. S. Banu, S. Das, T. Chattopadhyay, R. Sanyal, E. Zangrando and D. Das, *Polyhedron*, 2013, **52**, 669–678.

16. X. F. Hu and L. Wu, *Chemical Papers*, 2012, **66**, 211–215.

17. A. Vijayaraj, R. Prabu, R. Suresh, S. Sundaramoorthy, D. Velmurugan and V. Narayanan, *J Iran. Chem. Soc.*, 2013, **10**, 63–76.

18. *(a)* M. R. Maurya, N. Chaudhary, F. Avecilla and I. Correia, *J. Inorg. Biochem.*, 2015, **147**, 181–192; *(b)* M. R. Maurya, N. Kumar and N. Chaudhary, *Polyhedron*, 2015, **97**, 103–111.

19. R. A. Rowe and M. M. Jones, *Inorg. Synth.*, 1957, **5**, 113–116.

20. A. Rockenbauer and L. Korecz, *Appl. Magn. Reson.* 1996, **10**, 29–43.

21. *SHELX*, G. M. Sheldrick, Acta Crystallogr., Sect. A, 2008, **64**, 112–122.

22. G. M. Sheldrick, *SADABS*, version 2.10, University of Göttingen, Germany, (2004).

23. X. Lei and N. Chelamalla; *Polyhedron*, 2013, **49**, 244–251.

24. M. W. Makinen and M. Salehitazangi, *Coord. Chem. Rev.*, 2014, **279**, 1–22.

25. M. R. Maurya, M. Bisht, A. Kumar, M. L. Kuznetsov, F. Avecilla and J. Costa Pessoa, *Dalton Trans.*, 2011, **40**, 6968–6983.

26. M. R. Maurya, A. Arya, U. Kumar, A. Kumar, F. Avecilla and J. Costa Pessoa, *Dalton Trans.*, 2009, 9555–9566.

27. L.Vilas Boas, J. Costa Pessoa, *"Vanadium" in Comprehensive Coordination Chemistry*, ed. G. Wilkinson, R. D. Gillard and J. A. McCleverty, Pergamon, Oxford, 1987, Vol. 3, pp. 453–583.

28. F. Avecilla, P. Adão, I. Correia and J. Costa Pessoa, *Pure Appl. Chem.*, 2009, **48**, 1297–1311, 2009.

29. P. Adão, M. R. Maurya, U. Kumar, F. Avecilla, R. T. Henriques, M. L. Kusnetsov, J. Costa Pessoa and I. Correia, *Pure Appl. Chem.*, 2009, **81**, 1279–1296.

30. I. Correia, J. Costa Pessoa, M. T. Duarte, R. T. Henriques, M. Fátima M Piedade, L. F. Veiros, T. Jakusch, T. Kiss, Á. Dörnyei, M. C. A. Castro, C. F. G. C. Geraldes and F. Avecilla, *Chem. A. Eur. J.*, 2004, **10**, 2301–2317.

31. P. Adão, J. Costa Pessoa, R. T. Henriques, M. L. Kuznetsov, F. Avecilla, M. R. Maurya, U. Kumar and I. Correia, *Inorg. Chem.*, 2009, **48**, 3542–3561.

32. A. W. Addison, N. T. Rao, J. Reedijk, J. van Rijn and G. C. Verschoor, *J. Chem. Soc. Dalton Trans.*, 1984, 1349–1356.

33. M. M Hänninen, A. Peuronen, P. Damlin, V. Tyystajärvi, H. Kivelä and A. Lehtonen, *Dalton Trans.*, 2014, **43**, 14022–14028.

34. I. Cavaco, J. Costa Pessoa, M. T. Duarte, R.T. Henriques, P. M. Matias, R. D. Gillard, *J. Chem. Soc. Dalton Trans.*, 1996, 1989–1996.

35. J. Costa Pessoa, M. J. Calhorda, I. Cavaco, I. Correia, M. T. Duarte, V. Felix, R. T. Henriques, M. F. M. Piedade and I. Tomaz, *J. Chem. Soc. Dalton Trans.*, 2002, 4407–4415.

36. F. Wolff, C. Lorber, R. Choukroun and B. Donnadieu, *Inorg. Chem.*, 2003, **42**, 7839–7845.

37. *(a)* D. Rehder, C. Weidemann, A. Duch and W. Priebsch, *Inorg. Chem.*, 1988, **27**, 584–587; *(b)* W. Priebsch and D. Rehder, *Inorg. Chem.*, 1990, **29**, 3013–3019.

38. L. Pettersson, I. Andersson and A. Gorzás, *Coord. Chem. Rev.*, 2003, **237**, 77–87.

39. V. Conte, F. di Furia and S. Moro, *J. Mol. Cat.*, 1994, **94**, 323–333.

40. S. Funahashi, K. Ishihara, M. Inamo and M. Tanaka, *Inorg. Chim. Acta*, 1989, **157**, 65–71.

41. *(a)* V. Conte, F. D. Furia and S. More, *Inorg. Chim. Act.*, 1998, **172**, 62–47.; *(b)* C. Slebodnick and V. L. Pecoraro, *Inorg. Chim. Act.*, 1998, **283**, 37–43.

42. S. R. Cooper, Y. B. Koh and K. N. Raymond, *J. Am. Chem. Soc.*, 1982, **104**, 5092–5102.

43. *(a)* C. R. Cornman, G. J. Colpas, J. D. Hoeschele, J. Kampf and V. L. Pecoraro, *J. Am. Chem. Soc.*, 1992, **114**, 9925–9933, *(b)* C. L. Simpson and C. G. Pierpont, *Inorg. Chem.*, 1992, **31**, 4308–4313.

44. M. R. Maurya, M. Bisht, N. Chaudhary, A. Kumar, F. Avecilla and J. Costa Pessoa, *Eur. J. Inorg. Chem.*, 2012, 4846-4855.

45. M. E. Cass, D. L. Greene, R. M. Buchanan and C. G. Pierpont, *J. Am. Chem. Soc.*, 1983, **105**, 2680–2686.

46. M. E. Cass, N. R. Gordon and C. G. Pierpont, *Inorg. Chem.*, 1986, **25**, 3962–3967.

47. A. M. Nardillo and J. A. Catoggio, *Anal. Chim Acta*, 1975, **74**, 85–99.

48. P. J. Bosserman and D. T. Sawyer, *Inorg. Chem.*, 1982, **21**, 1545–1551.

49. Q. Lin, Q. Li, C. Batchelor–McAuley and R. G. Compton, *J. Phys. Chem. C*, 2015, **119**, 1489−1495.

50. X. Q. Zhu, C. H. Wang and H. Liang, *J. Org. Chem.*, 2010, **75**, 7240–7257.

51. E. J. Lien, S. Ren, H. H. Bui and R. Wang, *Free Radical Biology & Medicine*, 1999, **26**, 285–294.

52. *(a)* S. Kundu, D. Mondal, K. Bhattacharya, A. Endo, D. Sanna, E. Garribba and M. Chaudhury, *Inorg. Chem.*, 2015, **54**, 6203−6215; *(b)* B. Morgenstern, S. Steinhauser, K. Hegetschweiler, E. Garribba, G. Micera, D. Sanna and L. Nagy, *Inorg. Chem.* 2004, **43**, 3116−3126; *(c)* B. Morgenstern, B. Kutzky, C. Neis, S. Stucky, K. Hegetschweiler, E. Garribba and G. Micera, *Inorg. Chem.*, 2007, **46**, 3903−3915.

53. L. Pisano, K. Várnagy, S. Timári, K. Hegetschweiler, G. Micera and E. Garribba, *Inorg. Chem*. 2013, **52**, 5260−5272.

54. M. Branca, G. Micera, A. Dessi, D. Sanna and K. N. Raymond, *Inorg. Chem.*, 1990, **29**, 1586–1589.

55. M. Mba, M. Pontini, S. Lovat, C. Zonta, G. Bernardinelli, P. Kundig and G. Licini, *Inorg. Chem.* 2008, **47**, 8616–8618.

56. M. R. Maurya, S. Dhaka and F. Avecilla, *Polyhedron*, 2015, **96**, 79–87.

57. F. Sabuzi, E. Churakova, P. Galloni, R. Wever, F. Hollmann, B. Floris and V. Conte, *Eur. J. Inorg. Chem.*, 2015, http://dx.doi.org/10.1002/ejic.201500086.

58. D. Rehder, Bioinorganic Vanadium Chemistry, John Wiley & Sons, Chichester, 2008.

59. V. Conte, A. Coletti, B. Floris, G. Licini and C. Zonta, *Coord. Chem. Rev.*, 2011, **255**, 2165–2177.

60. *(a)* V. Conte, F. Di Furia and S. Moro, *J. Mol. Cat. A*, 1997, **117**, 139–149; *(b)* V. Conte, F. Di Furia and S. Moro, *J. Mol. Cat. A*, 1997, **120**, 93–99.